## ORIGINAL RESEARCH

Hepatic Autophagy Deficiency Remodels Gut Microbiota for Adaptive Protection via FGF15-FGFR4 Signaling

Shengmin Yan,[1,2] Bilon Khambu,[1,2] Xiaoyun Chen,[1] Zheng Dong,[3,4] Grace Guo,[5] and Xiao-Ming Yin[1,2]

[1]Department of Pathology and Laboratory Medicine, Indiana University School of Medicine, Indianapolis, Indiana; [2]Department of Pathology and Laboratory Medicine, Tulane University School of Medicine, New Orleans, Louisiana; [3]Department of Cell Biology and Anatomy, Medical College of Georgia at Augusta University, Augusta, Georgia; [4]Charlie Norwood VA Medical Center, Augusta, Georgia; and [5]Department of Pharmacology and Toxicology, Rutgers University, Piscataway, New Jersey
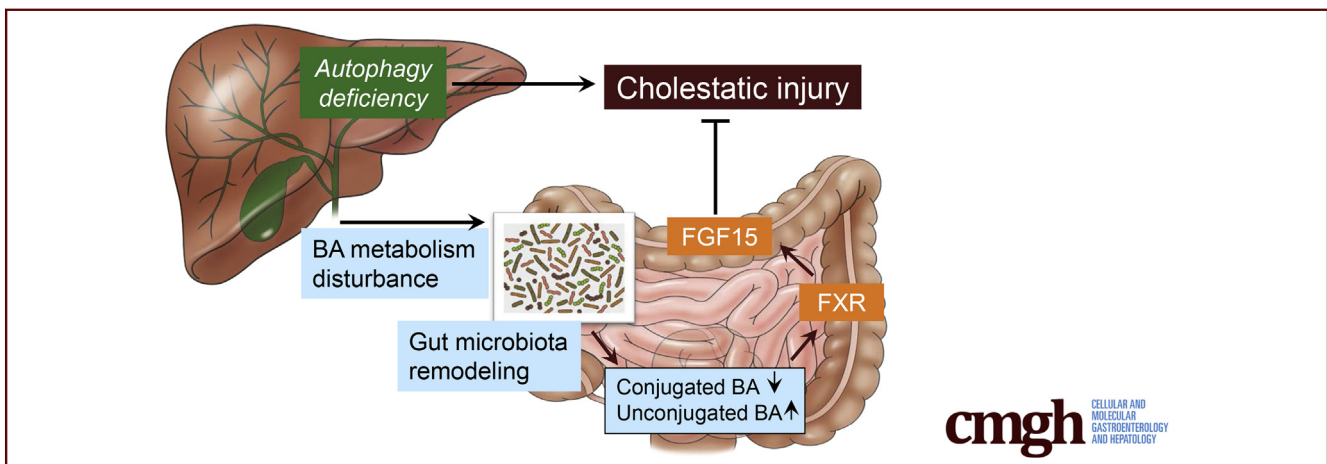
SUMMARY

Autophagy deficiency in the liver can cause alterations of intestinal bile acid (BA) composition and gut microbiota with a significantly higher proportion of BA-metabolizing bacteria. Gut dysbiosis provides an adaptive protection to the liver via the FGF15-FGFR4 signaling pathway.

BACKGROUND & AIMS: The functions of the liver and the intestine are closely tied in both physiological and pathologic conditions. The gut microbiota (GM) often cause deleterious effects during hepatic pathogenesis. Autophagy is essential for liver homeostasis, but the impact of hepatic autophagy function on liver-gut interaction remains unknown. Here we investigated the effect of hepatic autophagy deficiency (Atg5Δhep) on GM and in turn the effect of GM on the liver pathology.

METHODS: Fecal microbiota were analyzed by 16S sequencing. Antibiotics were used to modulate GM. Cholestyramine was used to reduce the enterohepatic bile acid (BA) level. The functional role of fibroblast growth factor 15 (FGF15) and ileal farnesoid X receptor (FXR) was examined in mice overexpressing FGF15 gene or in mice given a fibroblast growth factor receptor-4 (FGFR4) inhibitor.

RESULTS: Atg5Δhep causes liver injury and alterations of intestinal BA composition, with a lower proportion of tauro-conjugated BAs and a higher proportion of unconjugated BAs. The composition of GM is significantly changed with an increase in BA-metabolizing bacteria, leading to an increased expression of ileal FGF15 driven by FXR that has a higher affinity to unconjugated BAs. Notably, antibiotics or cholestyramine treatment decreased FGF15 expression and exacerbated liver injury. Consistently, inhibition of FGF15 signaling in the liver enhances liver injury.

CONCLUSIONS: Deficiency of autophagy function in the liver can affect intestinal environment, leading to gut dysbiosis. Surprisingly, such changes provide an adaptive protection against the liver injury through the FGF15-FGFR4 signaling. Antibiotics use in the condition of liver injury may thus have unexpected adverse consequences via the gut-liver axis. *(Cell Mol Gastroenterol Hepatol 2021;11:973–997; https://doi.org/10.1016/j.jcmgh.2020.10.011)*

Keywords: Autophagy; Gut Dysbiosis; Liver Injury; FGF15.

Gut microbiota (GM) consist of a diverse community of symbiotic bacteria and have a complex interplay with the host.[1] Interactions between GM and the host result in production of metabolites by microbes, including secondary bile acids (BAs).[1] Alteration of GM has been associated with multiple diseases, including fatty liver disease. Gut dysbiosis is found in patients with nonalcoholic fatty

liver disease (NAFLD) and nonalcoholic steatohepatitis.[2] In patients with alcohol-related liver disease, the microbiota composition and function are varied in association with the severity of liver condition and whether the patients are active drinkers.[3] On the other hand, gut dysbiosis may contribute to hepatic pathogenesis by translocation of microbial-associated molecular patterns and bacteria that can cross the gut barrier.[4] However, evidence of beneficial effects through a defined mechanism is scarce.

BAs are produced in hepatocytes through 2 major biosynthetic pathways, the classic pathway, which converts cholesterol to 7α-hydroxycholesterol by cytochrome P450 7A1 (CYP7A1), and the alternative pathway, which converts cholesterol to 27-hydroxycholesterol by cytochrome P450 27A1.[5,6] Eventually the classic pathway leads to the synthesis of cholic acid (CA) and chenodeoxycholic acid (CDCA), whereas the alternative pathway only leads to the synthesis of CDCA in mice.[5,6] In the human liver, CDCA is an end product; however, CDCA is further converted to muricholic acids (MCAs) by cytochrome P450 2C70 in the mouse liver.[5,6] Primary BAs are conjugated after synthesis and secreted to the intestine, where they are converted by GM into secondary BAs and reabsorbed by the liver through the portal circulation.[5,6] Dysfunction of BA metabolism and gut dysbiosis can be associated with each other, often in the context of liver diseases.[4,6] Gut dysbiosis has been found in patients with primary biliary cholangitis or primary sclerosing cholangitis and in a mouse model of cholestasis.[4,7] It is not known whether gut dysbiosis would in turn affect liver pathogenesis in the context of dysregulated BA metabolism.

Macroautophagy, hereafter simply referred to as autophagy, is an evolutionarily conserved degradation process and is critical for hepatic homeostasis.[8] Deficiency of key autophagy-related genes (Atg) in the liver, eg, Atg5 and Atg7, causes severe liver injury, fibrosis, and tumorigenesis.[9,10] Our previous study demonstrates that autophagy deficiency–induced liver injury is accompanied with altered hepatic BA metabolism, cholestatic injury, and impaired farnesoid X receptor (FXR) activity in the liver.[11] It is not known whether hepatic autophagy function can be important for the gut-liver interaction and exert its impact to the GM.

Our study shows that hepatic autophagy deficiency leads to an increased proportion of BA-metabolizing bacteria and the alteration of BA composition in the intestine. The significance of these changes is the enhanced activation of ileal FXR and an increased expression of fibroblast growth factor 15 (FGF15). Unexpectedly, we found an exacerbated liver injury and ductular reaction in autophagy-deficient livers after GM removal or blockage of the FGF15–fibroblast growth factor receptor 4 (FGFR4) signaling pathway. Our findings thus indicate that gut dysbiosis can be beneficial in protecting the liver from further injury, and the mechanism is medicated by a gut-liver signaling axis. Furthermore, the findings suggest that antibiotics (ABX) use in the condition of liver injury should be cautious, considering the potential adverse effect on the liver via the gut-liver signaling.

Results

Liver-Specific Deletion of Atg5 Altered the Composition of GM

Hepatic autophagy deficiency due to the deletion of a key autophagy gene, Atg5 or Atg7, causes significant liver injury, which is dependent on the nuclear factor erythroid 2-related factor 2 (NRF2) activation.[9,12,13] To investigate the impact of hepatic autophagy deficiency on GM, we first assessed the composition of GM in fecal samples from $Atg5^{F/F}$ and $Atg5^{\Delta hep}$ mice by 16S sequencing. Principal coordinates analysis (PCoA) showed that the composition of GM was noticeably separated between $Atg5^{F/F}$ and $Atg5^{\Delta hep}$ mice at the age of 8 or 16 weeks (Figure 1A). However, the diversity and the number of species were comparable between $Atg5^{F/F}$ and $Atg5^{\Delta hep}$ mice (Figure 1B). The most abundant bacteria at the phylum level were Bacteroidetes, Firmicutes, and Proteobacteria, and their proportions were in general comparable between $Atg5^{F/F}$ and $Atg5^{\Delta hep}$ mice (Figure 1C). These results suggest that hepatic Atg5 deletion alters the proportion of bacterial species rather than the diversity of GM. Analysis at the genus level showed significant disproportions of 8 bacteria between $Atg5^{F/F}$ and $Atg5^{\Delta hep}$ mice (Figure 1D). A higher proportion of Lactobacillus but a lower proportion of Prevotella, Paraprevotella, Turicibacter, Mogibacterium, and Ammonifex were observed in $Atg5^{\Delta hep}$ mice. The proportion of Johnsonella was also increased in most of the $Atg5^{\Delta hep}$ groups except the 16-week-old female group. In addition, Parapedobacter seemed enriched only in the male $Atg5^{\Delta hep}$ mice but impoverished in the females.

To understand whether the disproportion of GM was correlated with the autophagy deficiency, we analyzed GM in $Atg7^{\Delta hep}$ mice, another hepatic autophagy-deficiency mouse model. As observed in the $Atg5^{\Delta hep}$ mice, the diversity and the number of identified species were comparable between $Atg7^{\Delta hep}$ mice and their controls (Figure 2A and B). However, proportions of 9 genera were changed in
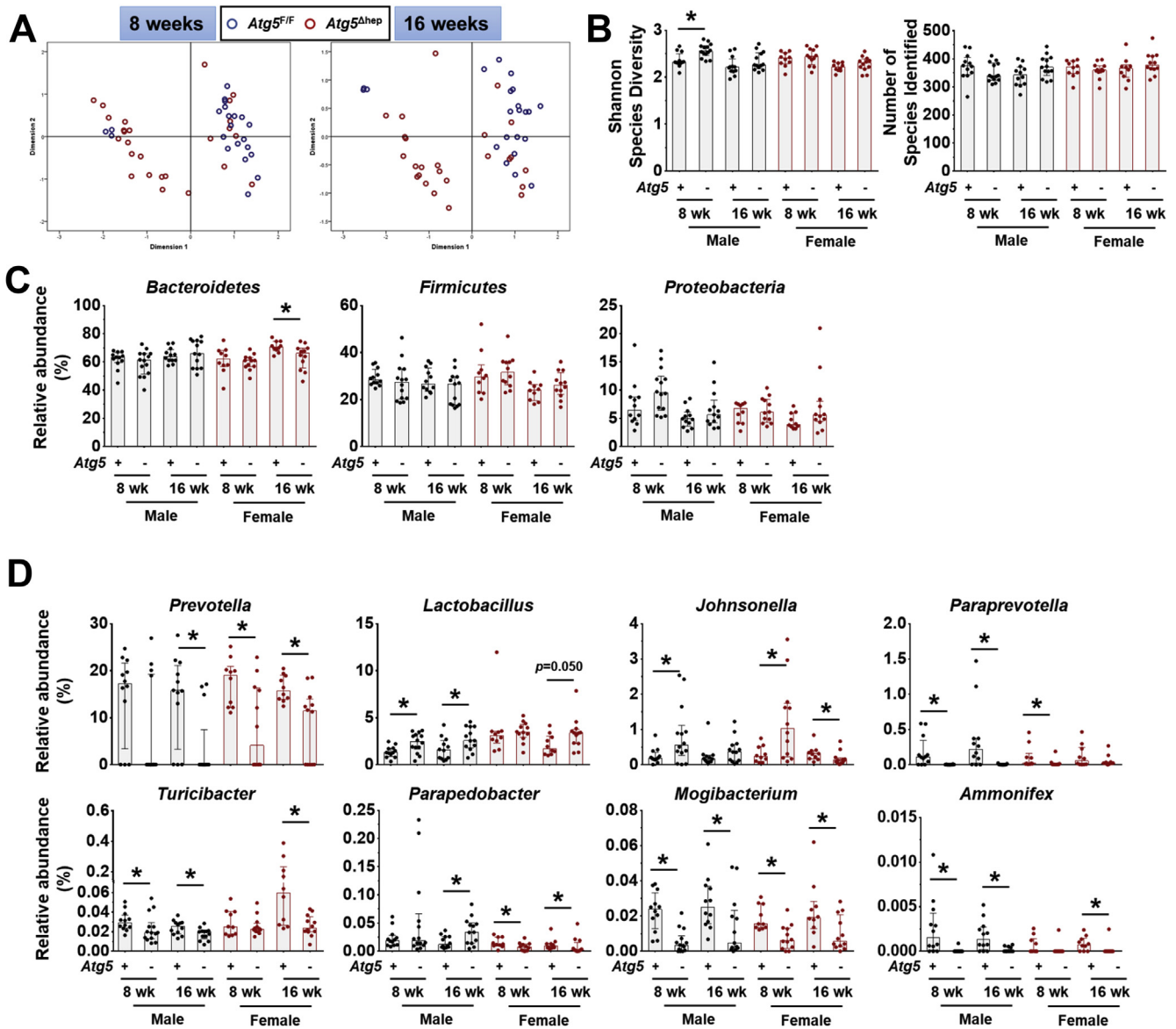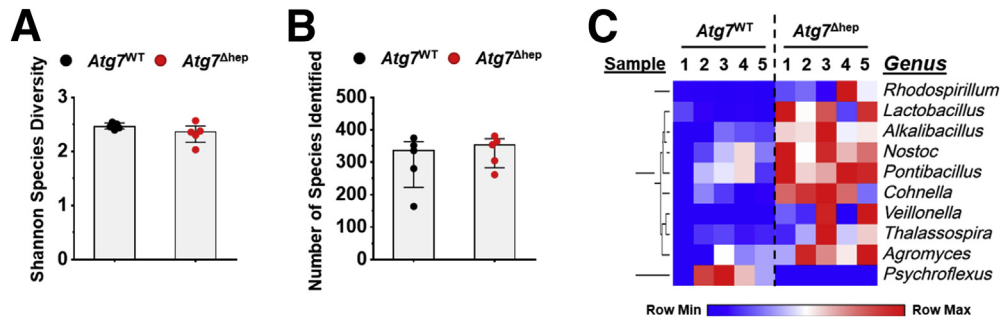
Figure 1. Liver-specific deletion of *Atg5* altered the composition of GM. (*A*) PCoA based on relative abundance at species level shows a distinguishable profile of GM between 8- and 16-week-old *Atg5^F/F^* and *Atg5^Δhep^* mice. Data from mice of both sexes were plotted. (*B*) Shannon species diversity and number of species identified were similar among different groups of mice. (*C*) Proportion of 3 most abundant bacteria at phylum level. (*D*) Proportion of bacteria that showed significant changes in at least 3 comparisons between the age- and sex- matched *Atg5^F/F^* and *Atg5^Δhep^* mice at the genus level. Data are shown as median with interquartile range, n = 10/group. Mann-Whitney analysis was used to determine significance, *$P < .05$.

*Atg7^Δhep^* mice (Figure 2*C*), including *Lactobacillus*. These results indicate that hepatic autophagy deficiency can cause gut dysbiosis.

ABX Treatment Aggravated Atg5 Deficiency-Induced Liver Injury

To investigate the potential impact of GM dysbiosis on the pathogenesis of hepatic autophagy deficiency, mice were given ABX for 6 weeks (Figure 3*A*). ABX treatment did not affect either hepatic NRF2 activity (Figure 4*A* and *B*), which could affect liver injury,[12] or water consumption

(Figure 4*C*). The hepatomegaly in *Atg5^Δhep^* mice remained unchanged after ABX treatment (Figure 3*B* and *C*). Nevertheless, gallbladders were enlarged after ABX treatment (Figure 3*B* and *C*), which is consistent with previous findings in germ-free mice.[14] Unexpectedly, serum levels of alanine transaminase (ALT), aspartate transaminase (AST), alkaline phosphatase (ALP), and total BA (TBA) were significantly increased in *Atg5^Δhep^* mice but not significantly changed in *Atg5^F/F^* mice after ABX treatment (Figure 3*D*). Consistently, ABX treatment enhanced ductular reaction but not fibrotic reaction as shown by H&E, cytokeratin 19 (CK19), and Masson's trichrome staining in *Atg5*-deficient

Figure 2. Liver-specific deletion of *Atg7* caused gut dysbiosis. Shannon species diversity (*A*) and the number of species identified (*B*) were analyzed in each group of mice. (*C*) Bacteria with disproportionate representation in *Atg7*$^{\Delta hep}$ mice at genus level. Heatmap was generated, and values in the heatmap were mapped to colors using the minimum and maximum of each row independently. The hierarchical cluster of different genus was constructed using one minus Pearson correlation method. Male and female mice were 6–26 weeks old when fecal samples were collected (n = 5). Data are shown as median with interquartile range. Mann-Whitney analysis did not show statistical significance between the groups.

livers (Figure 3*E*). Autophagy deficiency causes liver injury accompanied with cholestasis.[11] Consistently, *Atg5*$^{\Delta hep}$ mice presented increased TBA mainly in the liver and the feces (Figure 3*F*). ABX treatment caused further elevations in TBA levels mainly in the intestine and the gallbladder, and thus the TBA pool elevated in *Atg5*$^{F/F}$ mice but more so in *Atg5*$^{\Delta hep}$ mice (Figure 3*F*). Similar to germ-free mice, accumulation of TBA in the intestine was accompanied with decreased fecal levels of TBA after ABX treatment (Figure 3*F*). Overall, ABX treatment enhanced cholestatic liver injury of *Atg5*$^{\Delta hep}$ mice.

In *Atg7*$^{\Delta hep}$ mice, ABX treatment increased TBA in the intestine and the total pool while decreased fecal excretion of TBA (Figure 5*A*), the changes of which are similar to *Atg5*$^{\Delta hep}$ mice. However, hepatic enzyme levels in the blood were not further elevated in ABX-treated *Atg7*$^{\Delta hep}$ mice (Figure 5*B*). This could be due to the well-documented more severe liver injury seen in *Atg7*$^{\Delta hep}$ mice (Figure 5*B* and *C* vs Figure 3*C* and *D*). The more severe phenotype of *Atg7*-deficient livers may mask the effects of ABX treatment.

### BA-Metabolizing Bacteria Were Enriched in Atg5$^{\Delta hep}$ Mice

Because GM are critical for BA metabolism in the intestine,[15,16] we examined whether the disproportion of GM affected BA metabolism in *Atg5*$^{\Delta hep}$ mice. The major BA-metabolizing bacteria are those that express bile salt hydrolase (BSH) and/or 7α/β-dehydroxylation activity, which include *Lactobacillus*, *Bacteroides*, *Bifidobacterium*, *Eubacterium*, and *Clostridium*.[1] Of note, unlike BSH activity, only a small number of bacteria belonging to the class Clostridia have 7α/β-dehydroxylation activity.[17] A higher proportion of *Lactobacillus* (Figure 1*E*) but not *Clostridium* or *Eubacterium* (Figure 6*A*) was consistently found in *Atg5*$^{\Delta hep}$ mice. The elevation of *Bacteroides* was only observed in male *Atg5*$^{\Delta hep}$ mice, and that of *Bifidobacterium* was seen only in 16-week-old *Atg5*$^{\Delta hep}$ mice (Figure 6*A*). Thus, there were different levels of increments in BA-metabolizing bacteria in *Atg5*$^{\Delta hep}$ mice. In addition, we also observed an enrichment of *Lactobacillus* at genus level in *Atg7*$^{\Delta hep}$ mice (Figure 7*A*),

suggesting that hepatic autophagy deficiency altered proportions of BA-metabolizing bacteria.

Further heterogeneity at the species levels within each of these 5 genera could be observed in terms of the enrichment in *Atg5*$^{\Delta hep}$ mice. Because the variations could be related to the sex and/or the age, only a few species were overlapped between the cross-age/sex comparisons (Figure 8*A*). Two heatmaps based on the gender were then generated to include all disproportionate species, which presented the overall disproportion of the BA-metabolizing bacteria in *Atg5*$^{\Delta hep}$ mice (Figure 8*B*). As expected, most of these species with higher proportions were in both male and female *Atg5*$^{\Delta hep}$ mice, albeit with variations. We then focused on species that were disproportionately altered in both age-matched male and female *Atg5*$^{\Delta hep}$ mice. We found that among the 7 species that were altered in 8-week-old *Atg5*$^{\Delta hep}$ mice, 6 of them were enriched (Set 1 in Figure 6*B*). Similar enrichment of these species was seen in 16-week-old *Atg5*$^{\Delta hep}$ mice, although it was not statistically significant (Figure 6*B*). On the other hand, in the 16-week-old *Atg5*$^{\Delta hep}$ mice, 14 other species were disproportionate, and 13 of them were enriched (Set 2 in Figure 6*B*). We observed similar changes in *Atg7*$^{\Delta hep}$ mice. At species level, proportion of 9 species, including *Bifidobacterium thermophilum* and another 8 from genus *Lactobacillus*, was enriched in *Atg7*$^{\Delta hep}$ mice (Figure 7*B*). Overall, our results indicate that BA-metabolizing bacteria are enriched in hepatic autophagy-deficient mice at both genus and species levels, despite that there are age- and sex-related variations.

Liver-Specific Deletion of Atg5 Altered the Composition of Intestinal BAs

Because BA-metabolizing bacteria were enriched in *Atg5*$^{\Delta hep}$ mice, we interrogated the composition of BAs in the intestine and the liver. We found that the composition of intestinal BAs was distinctively separated among different groups (Figure 6*C* and *D*). In the intestine, the total level of unconjugated BAs was elevated, with a significant increase in CA in *Atg5*$^{\Delta hep}$ mice (Figure 6*E*). Correspondingly, most of the tauro-conjugated BAs, either primary or secondary,

A

B

C

D

E

F

Enterohepatic TBA
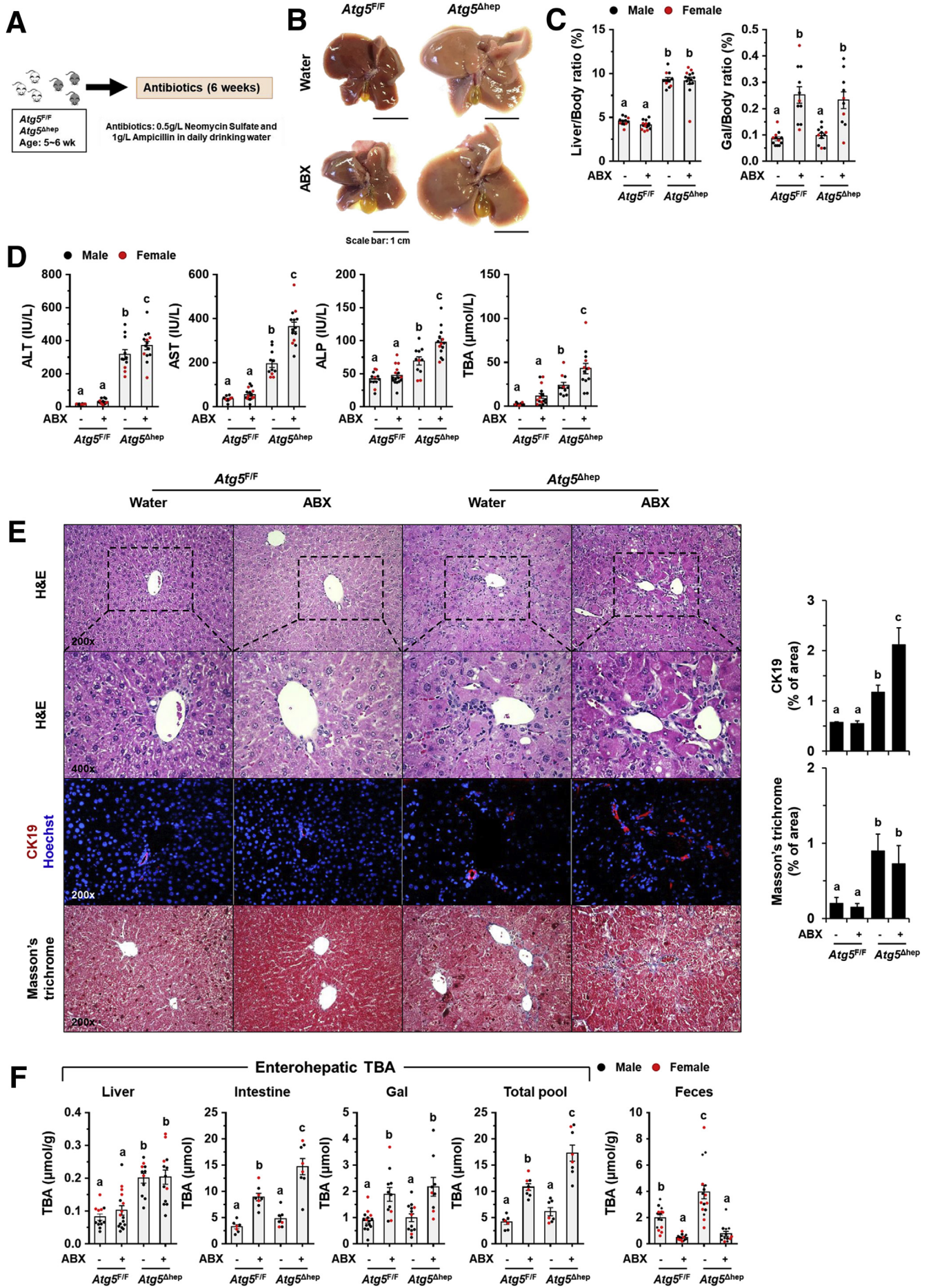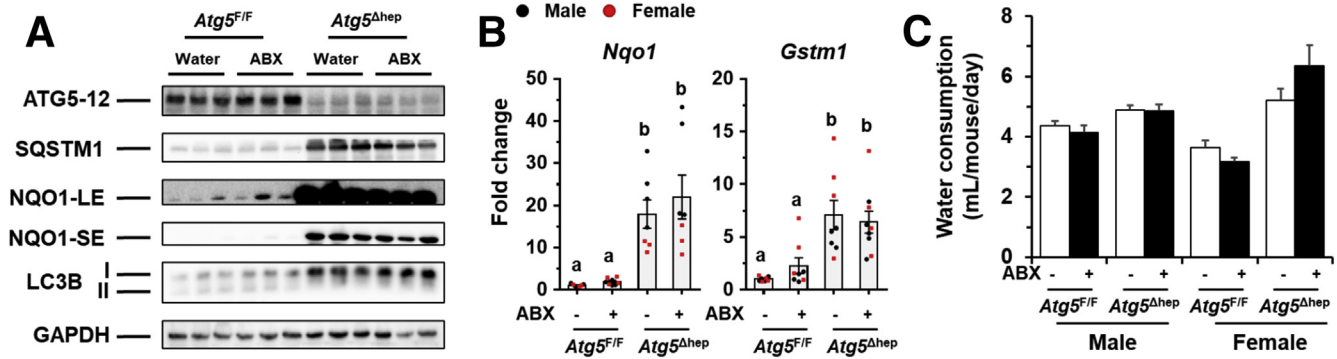
Figure 4. ABX treatment did not affect NRF2 activity in *Atg5* deficiency livers. (*A*) Immunoblotting analysis of hepatic samples. (*B*) The mRNA level of *Nqo1* and *Gstm1* was determined by qRT-PCR (n = 7–9). (*C*) Average daily water consumption per mouse was determined. Data are shown as means ± SE. Groups with different lowercase letters had significant differences (*P* < .05). *Gstm1*, glutathione s-transferase mu 1; *LC3B*, microtubule associated protein 1 light chain 3 beta; *Nqo1*, NAD(P)H quinone dehydrogenase 1.

were significantly reduced in $Atg5^{\Delta hep}$ mice (Figure 6*F*). The composition of intestinal BAs suggested a stronger capacity of deconjugation in $Atg5^{\Delta hep}$ mice. These observations are consistent with the higher proportion of BA-metabolizing bacteria in $Atg5^{\Delta hep}$ mice, which seemed to be more capable of deconjugation but not necessarily dehydroxylation. After ABX treatment, we observed that the proportion of unconjugated BAs was dramatically increased whereas the proportion of conjugated BAs was decreased in both $Atg5^{F/F}$ and $Atg5^{\Delta hep}$ mice (Figure 6*E* and *F*), the pattern of which is similar to the finding in germ-free mice.[14] Interestingly, *Atg5* deletion in the liver did not change the effects of ABX on intestinal composition of BAs, which nondiscriminately eliminated BA-metabolizing bacteria for both deconjugation and dehydroxylation capability.

We then examined what potential impact of *Atg5* deficiency and ABX treatment on hepatic BA compositions as comparisons. BA compositions in the liver were distinctly separable among the groups (Figure 9*A* and *B*). As expected, the major BA species in the liver were the primary conjugated BAs (Figure 9*C* and *D*). Whereas total levels of both tauro-conjugated and unconjugated BAs did not seem to be affected significantly, individual BA composition showed changes that were associated with *Atg5* deletion and/or ABX treatment. We observed a significant increase of taurocholic acid (TCA), but not tauromuricholic acid (TMCA), in *Atg5*-deficient livers (Figure 9*D*). Hepatic levels of taurochenodeoxycholic acid (TCDCA), tauroursodeoxycholic acid (TUDCA), taurodeoxycholic acid (TDCA), and taurolithocholic acid (TLCA) were all decreased by *Atg5* deletion (Figure 9*D*). After ABX treatment, hepatic levels of TCA and

TCDCA were significantly decreased in $Atg5^{F/F}$ but not in $Atg5^{\Delta hep}$ mice (Figure 9*D*). Hepatic levels of TMCA-($\alpha+\beta$) and MCA-β were significantly increased in $Atg5^{F/F}$ mice, which is similar to the case of germ-free mice,[14] whereas the change was not observed in $Atg5^{\Delta hep}$ mice (Figure 9*C* and *D*). These results suggest that hepatic composition of BAs is altered but is less sensitive to ABX treatment in $Atg5^{\Delta hep}$ mice.[11]

Ileal FXR Activation and FGF15 Expression Were Up-regulated in Atg5$^{\Delta hep}$ Mice in a Manner Dependent on GM

Intestinal level of TMCA was significantly reduced in $Atg5^{\Delta hep}$ mice, which meanwhile was significantly affected by GM as indicated by the robust elevation after ABX treatment (Figure 6*F*). Indeed, TMCA-β in the intestine is known to particularly inhibit ileal FXR, which is activated by TCA.[16] Accumulation of TMCA-β was found in germ-free mice and in conventional mice given ABX treatment, which dramatically inhibited ileal FXR, which thereby reduced expression of FGF15.[14] FGF15 is secreted into portal circulation to function as a hormone.[18] In the liver, FGF15 can inhibit BA synthesis when binding to its receptor FGFR4, which is critical for BA homeostasis.[19–23]

We therefore hypothesized that the lower level of intestinal TMCA in $Atg5^{\Delta hep}$ mice might allow a higher level of ileal FXR activation and a higher level of FGF15 expression. As expected, we found a significant increase of ileal expression of *Fgf15* and small heterodimer partner (*Shp*) in $Atg5^{\Delta hep}$ mice, which is compromised by ABX treatment

Figure 3. (*See previous page*). ABX treatment aggravated *Atg5* deficiency-induced liver injury. (*A*) Scheme of the ABX treatment. Mice were given neomycin sulfate and ampicillin sodium salt mixture in daily drinking water for 6 weeks. (*B*) Representative gross anatomy of livers of indicated genotypes and treatments. (*C*) Liver weight and gallbladder (Gal) weight were determined as percentages of the body weight (n = 10–16/group). (*D*) Serum levels of ALT, AST, ALP, and TBA in mice (n = 10–16/group). (*E*) Liver sections were subjected to H&E, anti-CK19, or Masson's trichrome staining. Percentage of positive area was quantified with ImageJ (anti-CK19 staining quantification, n = 3–4/group; Masson's trichrome staining quantification, n = 8–12/group). (*F*) TBA levels in indicated compartments were measured (n = 7–16/group). Data are shown as means ± SE. Groups with different lowercase letters had significant differences (*P* < .05).
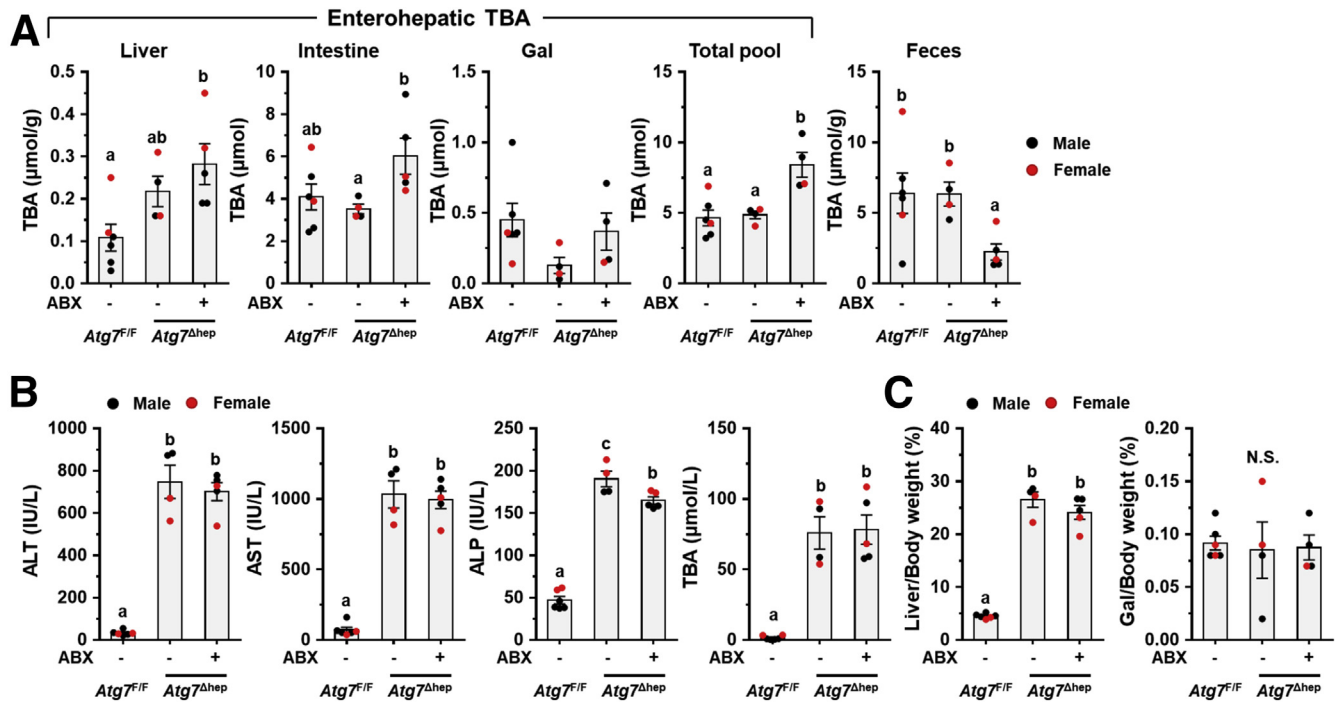
Figure 5. ABX treatment suppressed ileal FXR activity and altered enterohepatic TBA levels in *Atg7^Δhep* mice. (*A*) TBA levels in the indicated compartments were measured (n = 4–6). (*B*) Serum levels of ALT, AST, ALP, and TBA in *Atg7^Δhep* mice after ABX treatment (n = 4–6). (*C*) Liver weight and gallbladder (Gal) weight were shown as percentage of body weight (n = 4–6). Data are shown as means ± SE. Groups with different lowercase letters had significant differences (*P* < .05).

(Figure 10A), implying the involvement of TMCA. *Fxr* expression itself was not affected. In addition to *Fgf15* and *Shp*, expression of intestinal BA transporters, which is regulated by FXR,[24] is also affected by hepatic autophagy deficiency. In *Atg5^Δhep* mice, ileal expression of both ileal bile acid-binding protein (*Ibabp*) and organic solute transporter subunit-α (*Ost*)-α, but not *Ost-β*, was up-regulated, but compromised by ABX treatment (Figure 10A). Ileal apical sodium–bile acid transporter (*Asbt*) expression was noticeably decreased in *Atg5^Δhep* mice (Figure 10A). After ABX treatment, expression of *Mrp2* and *Asbt* was induced in mice of both genotypes (Figure 10A). The pattern of gene expression indicates that the activation of ileal FXR in *Atg5^Δhep* mice can be compromised by ABX treatment, suggesting a potential association of these changes with GM.

The elevation of ileal FGF15 expression was further confirmed by immunoblotting (Figure 10B and *C*) and immunochemistry (Figure 10D), both of which were increased in *Atg5^Δhep* mice in a manner dependent on GM. Interestingly, ileal expression of *Fgf15* and *Ibabp* was induced in *Atg7^Δhep* mice, which was also compromised after ABX treatment (Figure 11), suggesting that the modulation of ileal FXR activity by hepatic autophagy deficiency was not dependent on specific autophagy-related genes.

To examine the consequent impacts of FGF15 on *Atg5*-deficient livers, we analyzed FGF15-related pathways. In livers, FGF15 can bind to FGFR4 and activate the extracellular signal-regulated kinase (ERK) pathway.[19] As expected, phosphorylation level of ERK1/2 in *Atg5*-deficient livers was significantly induced but compromised after

ABX treatment (Figure 10E). *Cyp7a1* gene that encodes the rate-limiting enzyme in the classic BA synthesis pathway is negatively regulated by FGF15 signaling.[19] Indeed, whereas *Cyp7a1* mRNA level is low in *Atg5^Δhep* livers, its expression was noticeably elevated after ABX treatment (Figure 10F), which is similar to the case in the germ-free mice[14] and consistent with the alteration in the FGF15 signaling. Expression of *Fxr* and most of its target genes was suppressed in *Atg5*-deficient liver, as shown in our previous study,[11] but not affected by ABX treatment (Figure 12A and *B*).

Taken together, ABX treatment affects the intestinal composition of BA and eliminates the relative advantage of *Atg5^Δhep* mice in producing more ileal FGF15 because of a lower level of TMCA in the intestine.

Bile Acid Sequestrants Reduced TBA Pool but Also Ileal FGF15 Production, Leading to an Enhanced Atg5 Deficiency-Induced Liver Injury

Bile acid sequestrants (BAS) are large polymers that bind negatively charged BAs in the small intestine, which can prevent reabsorption of BAs in the gut, increase their fecal excretion, and finally disrupt enterohepatic circulation.[25] BAS are efficient to reduce TBA pool; however, evidence also has shown that they can consequently inhibit ileal FXR and reduce expression of FGF15 in mice[26] and FGF19 in humans.[19] To determine the impact of enterohepatic TBA on autophagy-deficient livers, mice were given cholestyramine resin treatment (Figure 13A). As expected, a
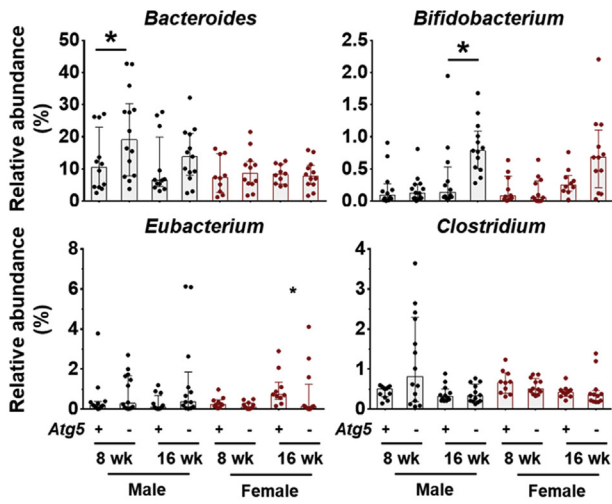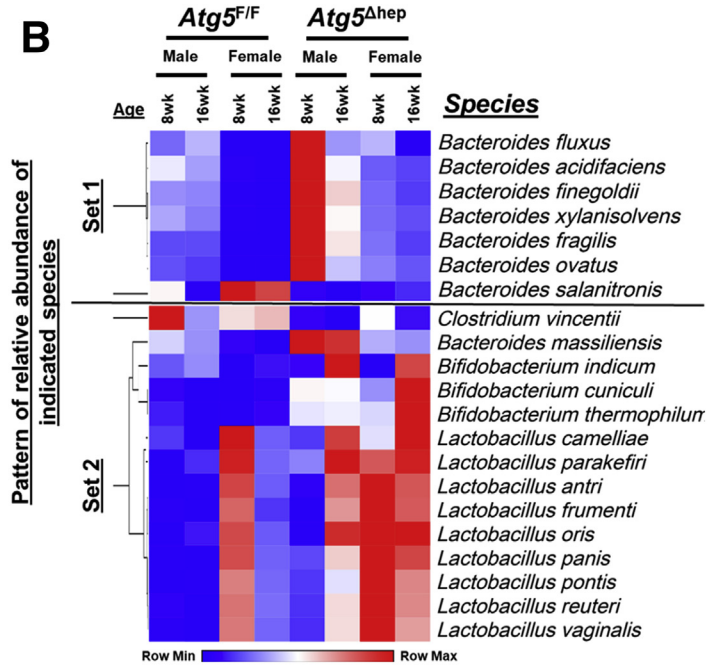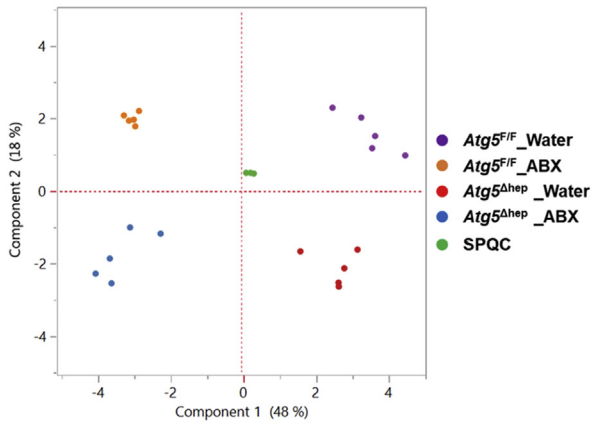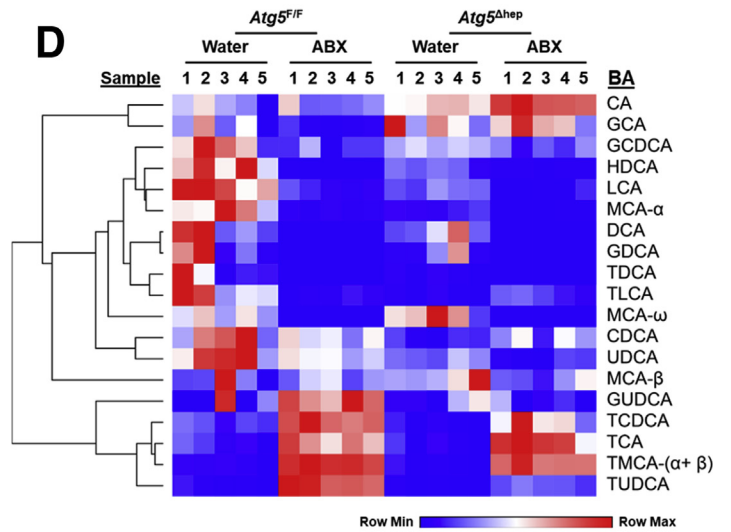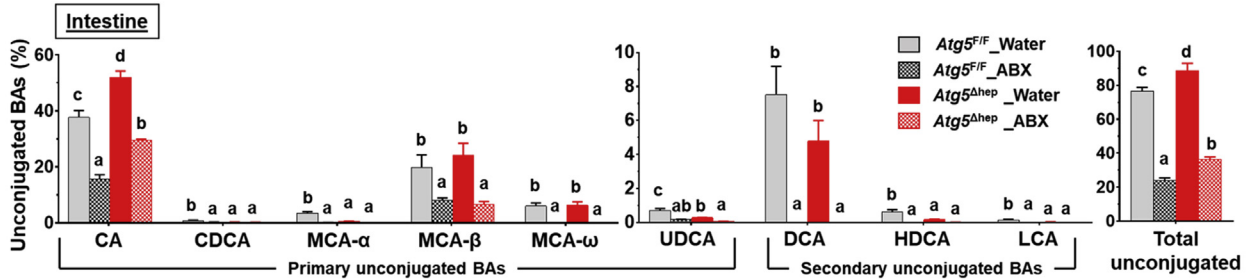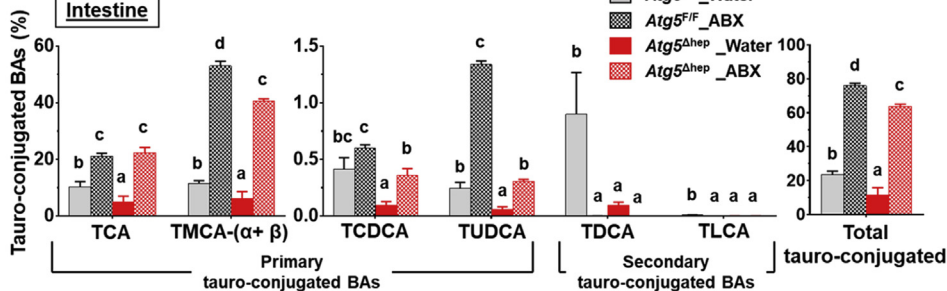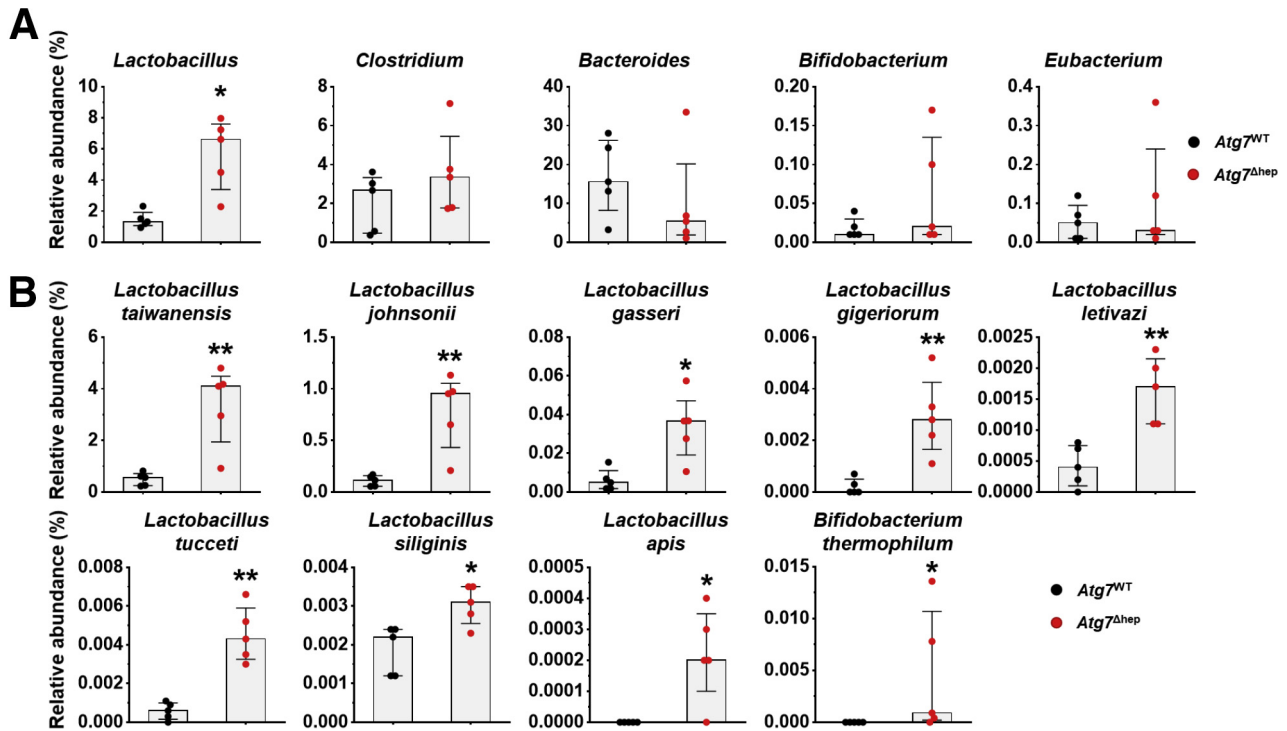
Figure 7. Alterations in the proportion of BA-metabolizing bacteria in Atg7$^{\Delta hep}$ mice. (*A*) Proportion of bacteria with BSH and/or $7\alpha/\beta$-dehydroxylation activity at the genus level in floxed *Atg7* or in *Atg7*$^{\Delta hep}$ mice. Mice were 6–26 weeks old. Both male and female mice were included. (*B*) The bacterial species with BSH and/or $7\alpha/\beta$-dehydroxylation activity that were disproportionate in *Atg7*$^{\Delta hep}$ mice. Data are shown as median with interquartile range, n = 5. Mann-Whitney analysis, *$P < .05$, **$P < .01$.

significant decrease of TBA levels in livers and enterohepatic circulation (Figure 13*B*) and reduced gallbladder size (Figure 13*C*) were observed in mice after BAS treatment. Although hepatomegaly in *Atg5*$^{\Delta hep}$ mice was not further enhanced (Figure 13*C*), serum levels of ALT, AST, and ALP were all increased in *Atg5*$^{\Delta hep}$ mice after BAS treatment (Figure 13*D*). H&E staining showed an increased number of oval cells around the periportal areas in *Atg5*-deficient livers after BAS treatment (Figure 13*E*). The increased positive areas of CK19 and Masson's trichrome staining indicate a more severe ductular reaction in *Atg5*-deficient livers after BAS treatment (Figure 13*E*). These

results suggest that BAS treatment in *Atg5*$^{\Delta hep}$ mice paradoxically enhances liver injury.

To identify potential mechanisms in which BAS treatment contributed to enhanced liver injury in *Atg5*$^{\Delta hep}$ mice, we examined expression of FXR-regulated genes in both ileums and livers. Despite an increase of *Fxr* gene expression in *Atg5*$^{F/F}$ mice after BAS treatment, ileal expression of FXR-promoted genes, including *Fgf15*, *Shp*, *Ibabp*, *Ost-α*, and *Ost-β*, was significantly reduced in mice after BAS treatment (Figure 13*F*). The ileal level of *Asbt* mRNA, an FXR-suppressed gene, was increased after BAS treatment (Figure 13*F*). These results suggested that ileal FXR activity

---

Figure 6. (*See previous page*). **Hepatic autophagy deficiency affects intestinal BA composition in correlation with gut dysbiosis.** (*A*) Hepatic autophagy deficiency affected the proportion of bacteria with the BSH and/or $7\alpha/\beta$-dehydroxylation activities at the genus level (*Lactobacillus* is shown in Figure 1*E*). Data are shown as median with interquartile range, n = 10/group. (*B*) Heatmap shows the BA-metabolizing bacteria that are disproportionate in *Atg5*$^{\Delta hep}$ mice at the species level. Heatmap was generated, and values in the heatmap were mapped to colors using the minimum and maximum of each row independently. The hierarchical cluster of different species was constructed using one minus Pearson correlation method. Proportion of bacteria in Set 1 was significantly changed in both male and female *Atg5*$^{\Delta hep}$ mice at 8 weeks old. Proportion of bacteria in Set 2 was significantly changed in both male and female *Atg5*$^{\Delta hep}$ mice at 16 weeks old. (*C*) PCoA of BAs in the intestine data (log2-scaled µmol/L). (*D*) Heatmap was generated, and values in the heatmap were mapped to colors using the minimum and maximum of each row independently. Heatmap shows the cluster of indicated BA species in the intestine of different groups of mice. The hierarchical cluster of different BAs was constructed using one minus Pearson correlation method. (*E* and *F*) Intestinal levels of unconjugated (*E*) and tauro-conjugated (*F*) BAs in male mice. Data are shown as percentage of TBA level (means ± SE), n = 5/group. Groups with different lowercase letters or indicated by asterisk had significant differences ($P < .05$). HDCA, hyodeoxycholic acid; LCA, lithocholic acid; UDCA, ursodeoxycholic acid.
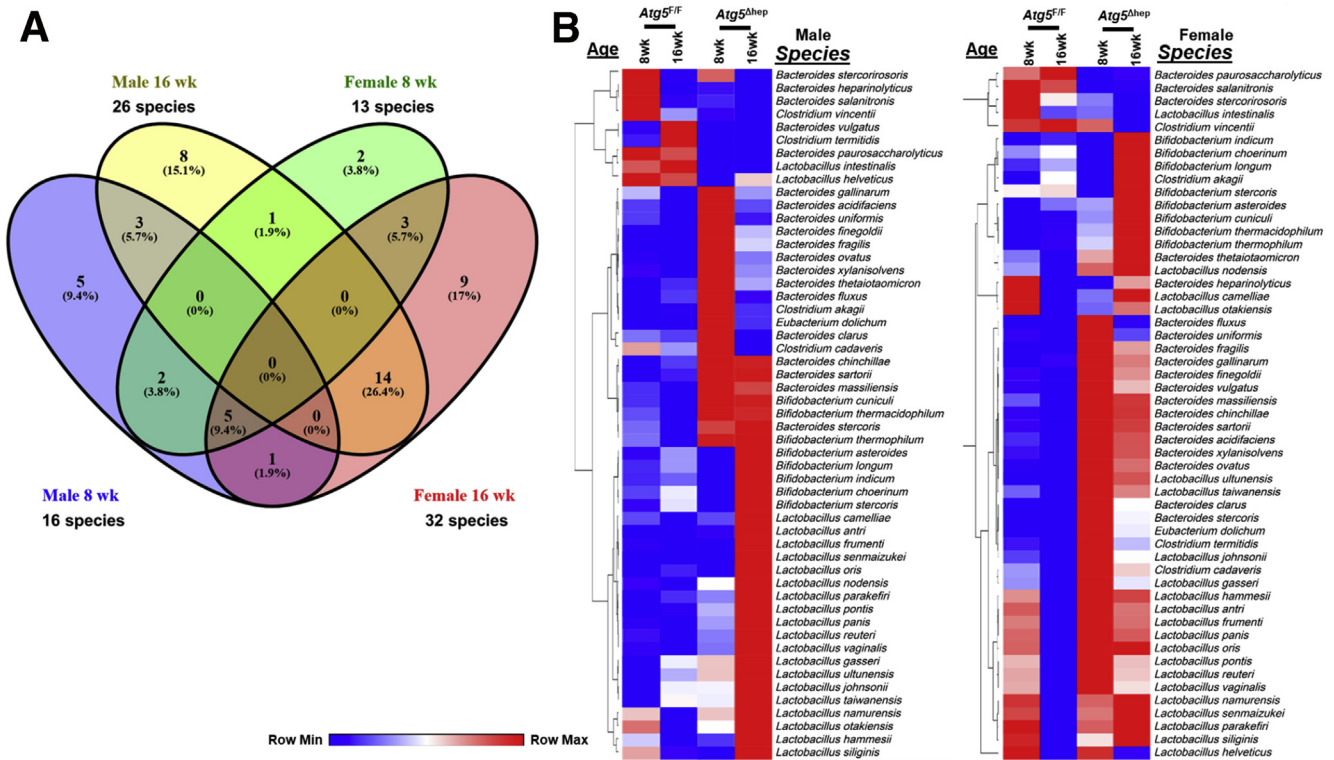
Figure 8. Hepatic autophagy deficiency caused changes in the proportion of BA-metabolizing bacteria. (*A*) Venn diagram shows the number of bacterial species with BSH and/or $7\alpha/\beta$-dehydroxylation activity, which were disproportionate in $Atg5^{\Delta hep}$ mice compared with the sex- and age- matched $Atg5^{F/F}$ mice. (*B*) Disproportionate bacteria at the species level were segregated on the basis of gender of the mouse. Heatmap was generated, and values in the heatmap were mapped to colors using the minimum and maximum of each row independently. The hierarchical cluster of different species was constructed using one minus Pearson correlation method.

was strongly inhibited by BAS treatment and consequently decreased expression of ileal *Fgf15*. In the liver, BAS treatment suppressed hepatic FXR activity in $Atg5^{F/F}$ mice but did not significantly change the expression of FXR targets in $Atg5^{\Delta hep}$ mice (Figure 13*G*), perhaps because the FXR activity was already reduced in autophagy-deficient livers. Taken together, these results suggest that BAS treatment in $Atg5^{\Delta hep}$ mice reduces ileal FXR activation and *Fgf15* expression, which may contribute to the paradoxical effects on autophagy deficiency–induced liver injury.

Intestine-Specific FXR Agonist Activated Ileal FXR in Atg5^F/F Mice but not in Atg5^Δhep Mice

Because both ABX and BAS treatments exacerbate liver injury in $Atg5^{\Delta hep}$ mice accompanied with reduced ileal FXR activity, we asked whether further activated ileal FXR can improve *Atg5* deficiency-induced liver injury. Hence, mice were given an intestine-specific FXR agonist, fexaramine (FEX), for 7 days (Figure 14*A*). Unexpectedly, FEX treatment did not change serum levels of ALT, AST, ALP, and TBA in $Atg5^{\Delta hep}$ mice, whereas serum level of TBA was decreased in $Atg5^{F/F}$ mice (Figure 14*B*). Analysis of the expression of ileal *Fxr* and its target genes suggested an activation of FXR in $Atg5^{F/F}$ mice but not in $Atg5^{\Delta hep}$ mice after FEX treatment (Figure 14*C*). The TBA pool and fecal TBA level were both

significantly reduced in $Atg5^{F/F}$ mice after FEX treatment, but not so much in $Atg5^{\Delta hep}$ mice (Figure 14*D*). We suspect that the lack of the effect of FEX in $Atg5^{\Delta hep}$ mice may be due to the altered GM and saturated FXR with existing BA agonists. Consistently, a prior study had also shown that GM could influence the efficacy of FEX treatment.[27]

Overexpression of FGF15 Attenuated Pathologic Features in Atg5^Δhep Livers

FGF15 was significantly induced in $Atg5^{\Delta hep}$ mice but was reduced after treatments with ABX or BAS. We thus hypothesized that an elevated level of FGF15 could play a protective role in *Atg5* deficiency-induced liver injury. Because recombinant FGF15 does not seem stable in the circulation for long-term experimentation,[28,29] AAV8-FGF15 was given to $Atg5^{\Delta hep}$ mice (Figure 15*A*). The level of phosphorylated ERK1/2 in the liver was elevated after AAV8-FGF15 injection 1 week and 4 weeks later (Figure 15*B*), suggesting that FGF15 signaling was enhanced in the liver as supported by a higher hepatic expression of *Fgf15* mRNA (Figure 15*C*). The protein level of FGF15 overexpression could not be defined because of lack of proper antibodies (data not shown). Consequently, hepatic levels of 2 classic targets of FGF15 signaling, *Cyp7a1* and cytochrome p450 family 8b1 (*Cyp8b1*), were reduced after
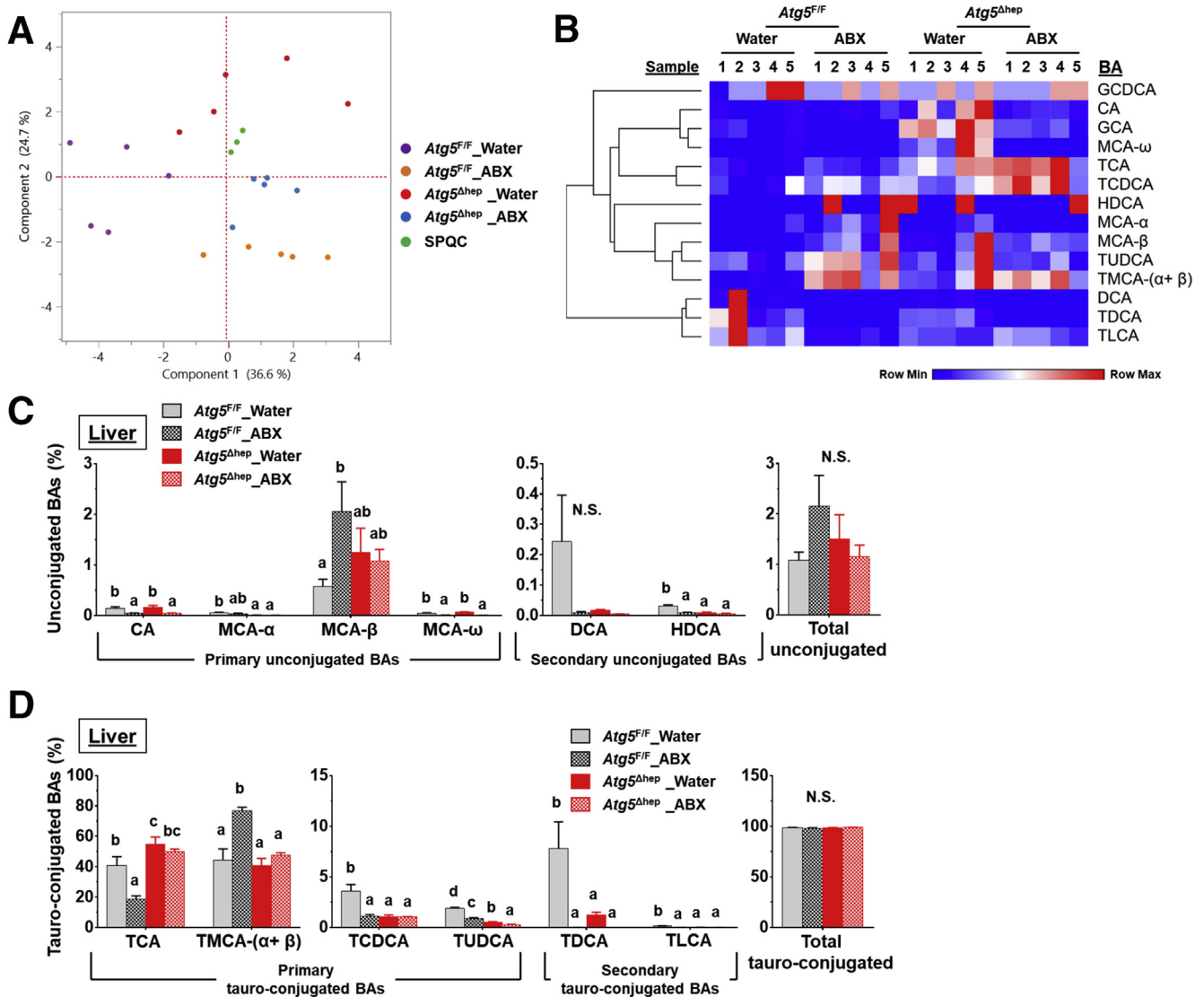
Figure 9. BA composition in the liver after ABX treatment. (*A*) PCoA of BAs in the liver (log2-scaled μmol/L). (*B*) Heatmap was generated, and values in the heatmap were mapped to colors using the minimum and maximum of each row independently. The hierarchical cluster of different BAs was constructed using one minus Pearson correlation method. (*C* and *D*) Hepatic levels of unconjugated BAs (*C*) and hepatic levels of tauro-conjugated bile acids (*D*) in male mice (n = 5). Data are shown as means $\pm$ SE. Groups with different lowercase letters had significant differences (*P* < .05). HDCA, hyodeoxycholic acid; LCA, lithocholic acid; UDCA, ursodeoxycholic acid.

FGF15 overexpression (Figure 15*C*). Paradoxically, hepatic *Fxr* and *Shp* expression was not elevated after FGF15 overexpression, although the expression of bile salt export pump (*Bsep*), a direct target of FXR, was induced (Figure 15*C*), suggesting FXR-independent effects of FGF15 on hepatic gene expression. Consistent with the reduced expression of *Cyp7a1* and *Cyp8b1*, the total TBA pool, mainly contributed by the intestinal level of BA, and the fecal TBA level were significantly reduced (Figure 15*D*).

Serum biochemistry analysis suggested FGF15 overexpression in the liver reduced ALP but not ALT, AST, and TBA (Figure 15*E*) in *Atg5*^Δhep^ mice, suggesting a potential improvement in biliary injury. Consistently, the H&E staining and CK19 staining showed a reduced ductular reaction

(Figure 15*F*). On the other hand, the parameters of fibrosis (Figure 16) showed a variable improvement to FGF15 overexpression, suggesting that the short treatment had a minor impact on this process.

Inhibition of FGFR4 Aggravated Liver Injury in Atg5^Δhep^ Mice

FGFR4 is the receptor that mediates FGF15 signaling in the liver.[19] To determine the role of FGF15-FGFR4 signaling in autophagy-deficient livers, we treated mice with Blu-9931 (BLU), a novel small molecular that selectively inhibits FGFR4,[30] to block FGFR4 activity (Figure 17*A*).

In both *Atg5*^F/F^ and *Atg5*^Δhep^ mice, BLU treatment reduced *Shp* expression, whereas it induced *Cyp7a1*
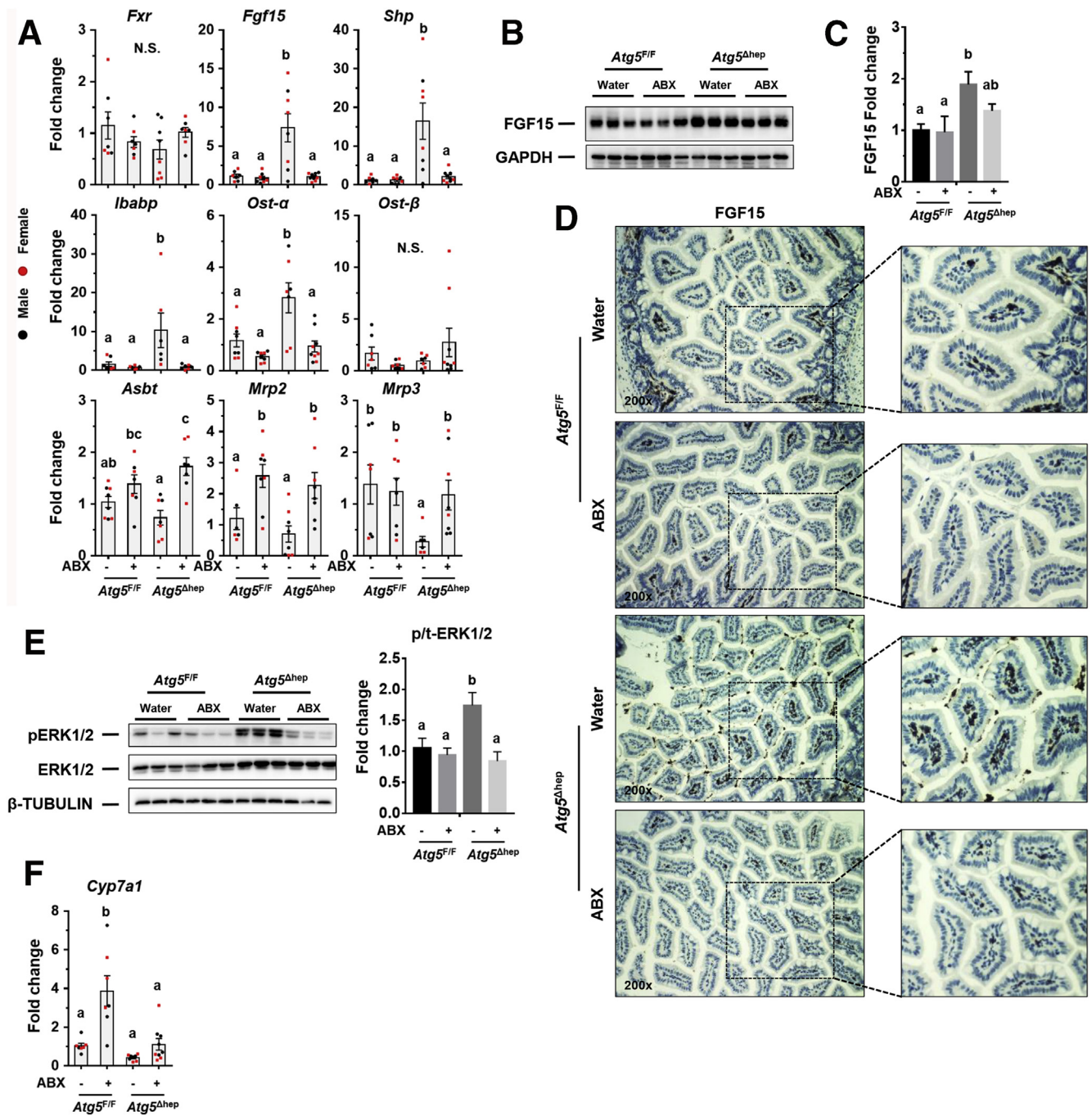
Figure 10. GM regulates ileal FXR activation and FGF15 expression in *Atg5^Δhep* mice. (*A*) mRNA level of indicated genes in the ileum was analyzed by qRT-PCR (n = 7–9/group). (*B* and *C*) Ileal FGF15 protein levels were examined by immunoblotting assay (*B*) and quantified with densitometry (*C*, n = 3/group). (*D*) Representative images of anti-FGF15 immunohistochemistry staining in the ileum of indicated genotypes and treatments. (*E*) ERK1/2 level in the liver was analyzed by immunoblotting assay and quantified by densitometry. Phosphorylation level of ERK1/2 was normalized by the total protein level and expressed as the fold change of the *Atg5^F/F* control group (n = 5–7/group). (*F*) Expression of *Cyp7a1* was analyzed by qRT-PCR in the liver (n = 6–9/group). Data are shown as means ± SE. Groups with different lowercase letters had significant differences (*P* < .05). *Mrp2* (*Abcc2*), multidrug resistance-associated protein 2; *Mrp3* (*Abcc3*), multidrug resistance-associated protein 3; N.S., no statistical significance.

expression in the liver (Figure 17*B*). Consequently, the TBA pool and fecal TBA level were significantly increased after BLU treatment (Figure 17*C*), indicating an increase of BA synthesis in the liver. Consistently, with the inhibition of

hepatic FGFR4, ileal expression of *Fgf15* and *Ibabp* was remarkably induced after BLU treatment (Figure 17*D*), which is possibly attributed to the increase of intestinal TBA.
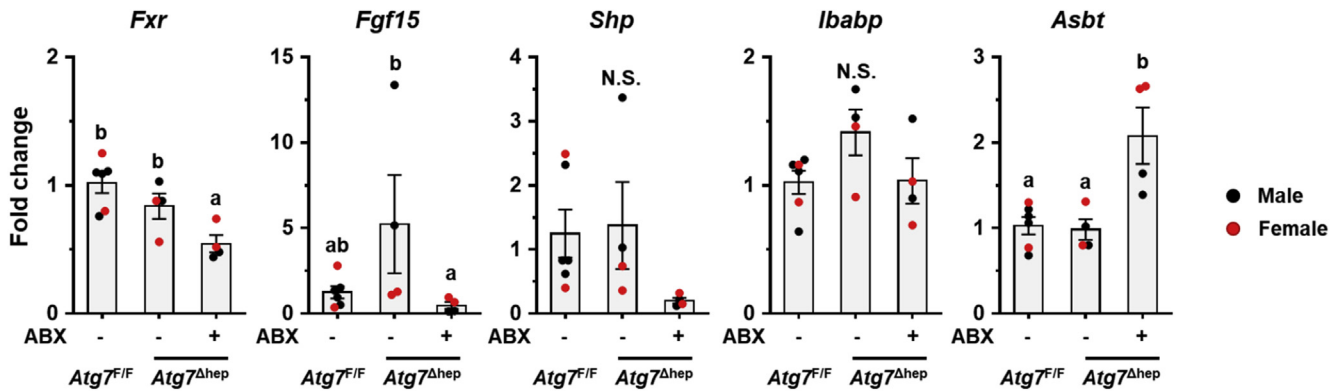
Figure 11. ABX treatment suppressed ileal FXR activity and reduced *Fgf15* expression in *Atg7*$^{\Delta hep}$ mice. Ileal expression of indicated genes was analyzed by qRT-PCR (n = 4–6). Data are shown as means $\pm$ SE. Groups with different lowercase letters had significant differences ($P < .05$).

After BLU treatment, liver injury was enhanced in *Atg5*$^{\Delta hep}$ mice as indicated by the significantly elevated serum levels of ALT, AST, and TBA (Figure 17*E*). Notably, the male mice were more susceptible to BLU treatment for the serum enzyme activation (Figure 18). We did not see significant pathologic changes in livers of *Atg5*$^{F/F}$ mice (Figure 17*F*), suggesting that inhibition of FGFR4 was not toxic in healthy livers. However, the ductular reaction around the periportal areas was further enhanced in *Atg5*-deficient livers after BLU treatment as indicated by H&E staining and the positive areas of CK19 staining (Figure 17*F*). Positive staining of Masson's trichrome was also significantly increased in *Atg5*-deficient livers after BLU treatment (Figure 17*F*). Although we found a noticeable sexual disparity in serum enzyme changes, changes in histologic studies were comparable between male and female *Atg5*$^{\Delta hep}$ mice. Taken together, these results suggest that FGF15-FGFR4 signaling protects livers from further injury in *Atg5*-deficient mice.

Discussion

### Interaction Between GM and Hepatic Autophagy Deficiency and BA Metabolism

In this study, we showed that autophagy deficiency in the liver led to the alteration of intestinal BA composition and gut dysbiosis with a significantly higher proportion of BA-metabolizing bacteria. Unexpectedly, ABX treatment increased enterohepatic level of BAs and exacerbated the pathology in autophagy-deficient livers. Together with other evidence, we demonstrate that enhanced activation of ileal FXR-FGF15 signaling, because of the effects of altered BA metabolism and GM, accounted for the protection of the autophagy-deficient liver from further injury (Figure 19). Therefore gut dysbiosis in liver diseases can be an adaptive response to mitigate the injury via a gut-liver signaling pathway.

Autophagy deficiency in the liver causes hepatomegaly, chronic injury, and tumorigenesis.[9,10] Mechanically, consistent activation of NRF2 by sequestosome-1 (SQSTM1) is critical for pathologic changes induced by hepatic *Atg5* or

Atg7 deletion,[9,12,13] yet how SQSTM1-NRF2 signaling leads to hepatocyte death remains unclear. Our previous study shows a compromised FXR activity and altered BA homeostasis in autophagy-deficient livers,[11] in which activation of FXR in the liver can ameliorate autophagy deficiency–induced liver injury, suggesting that reduced hepatic FXR expression and disrupted BA homeostasis may at least partially contribute to injury in autophagy-deficient livers.

In this study we have defined a unique interaction between GM and liver injury in the context of autophagy deficiency, which affects BA metabolism and gut-liver signaling. First, we show that dysfunction of BA metabolism induced by *Atg5* or *Atg7* deficiency in the liver alters GM and leads to a significant enrichment of BA-metabolizing bacteria with BSH activity. GM is critical for BA metabolism by deconjugation of BAs and conversion of primary BAs into secondary BAs.[6] Consistent with enriched BA-metabolizing bacteria, we observed a lower level of tauro-conjugated BAs but a higher level of unconjugated BAs in the intestine. However, levels of most secondary BAs in the intestine are lower in *Atg5*$^{\Delta hep}$ intestines except deoxycholic acid (DCA). In mice, DCA is converted from TCA, whereas other secondary BAs are converted from TCDCA.[31] Interestingly, TCDCA level is decreased in *Atg5*$^{\Delta hep}$ livers, suggesting a reduced capability of CDCA synthesis in these mice, which may contribute to the decreased levels of non-DCA secondary BAs in the intestine. Overall, the evidence here suggests that autophagy deficiency in the liver alters hepatic BA metabolism, which generates a different BA profile and favors the growth of a specific set of GMs. Thus the altered BA metabolism is the link connecting hepatic autophagy deficiency to gut dysbiosis.

Interestingly there are several studies indicating that GM are altered in patients with cholestatic liver diseases.[32–34] Several bacteria are consistently enriched in patients with primary biliary cholangitis or primary sclerosing cholangitis, including *Veillonella*, *Streptococcus*, *Enterococcus*, *Lactobacillus*, *Haemophilus*, and *Fusobacterium*, whereas the proportion of some other bacteria are decreased in these patients, such as *Phascolarctobacterium*, *Faecalibacterium*,
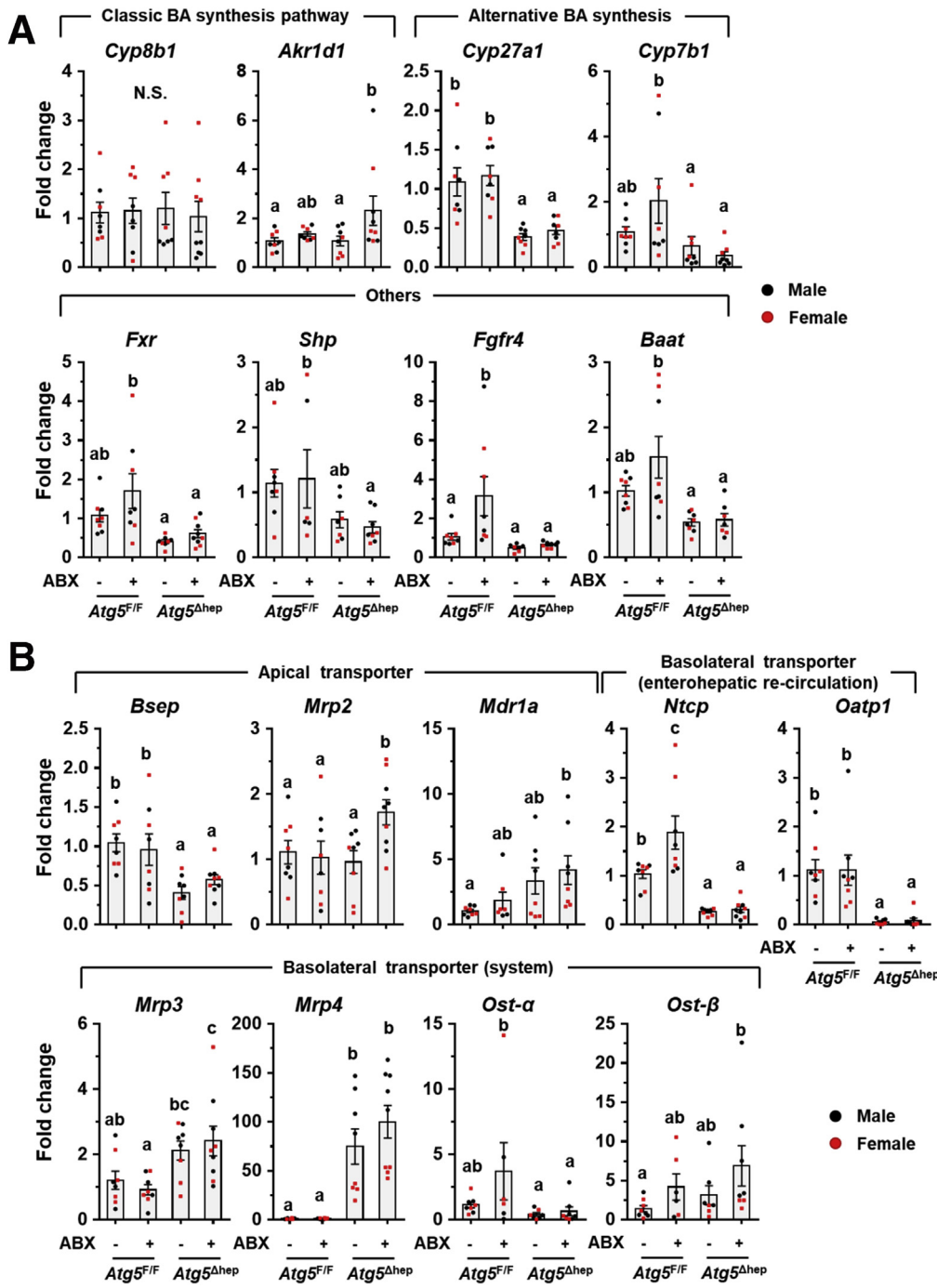
Figure 12. The mRNA level of hepatic genes related to BA metabolism after ABX treatment. (*A*) Expression of BA metabolism-related genes was analyzed by qRT-PCR in the liver (n = 6–9). (*B*) Hepatic expression of BA transporters was analyzed by qRT-PCR (n = 6–9). Data are shown as means ± SE. Groups with different lowercase letters had significant differences. Akr1d1, aldo-keto reductase family 1 member d1; Baat, bile acid-coa:amino acid n-acyltransferase; *Bsep* (*Abcb11*), bile salt export pump; *Cyp7b1*, cytochrome P450 7b1; *Cyp27a1*, cytochrome P450 27a1; *Mdr1a* (*Abcb1*), multidrug resistance protein 1; *Mrp2* (*Abcc2*), multidrug resistance-associated protein 2; *Mrp3* (*Abcc3*), multidrug resistance-associated protein 3; *Mrp4* (*Abcc4*), multidrug resistance-associated protein 4; *Ntcp* (*Slc10a1*), Na/Taurocholate cotransporting polypeptide; *Oatp1* (*Slco1a1*), organic anion-transporting polypeptide 1.

and *Blautia*. These findings indicate that some GM can be altered by cholangitis regardless of etiologies. In comparison, our data showed that *Lactobacillus* was elevated consistently in multiple groups of mice across the age and the sex at the genus level (Figures 1*D*, 2*C*, 7*A*) and at the species level (Figures 6*B*, 7*B*). In addition, *Streptococcus* and *Enterococcus* had shown some changes in some groups of Atg5Δhep mice, although not as consistently as *Lactobacillus* across the age and the sex (data not shown). Overall there is a notable similarity between the human cholestatic

injury and the autophagy deficiency–induced cholestatic injury in terms of gut dysbiosis.

Second, we found that altered GM maintain the enterohepatic BA level. We have reported cholestatic injury in autophagy-deficient livers, with a significant increase of TBA levels in serum and livers.[11] Here we not only confirmed our previous findings but also found that despite the increase of hepatic TBA level, the total TBA pool is comparable between the autophagy-deficient mice and the control mice (Figures 3*F*, 5*A*). This may be due to increased fecal

Figure panels A–G showing enterohepatic total bile acid (TBA) measurements, liver and gallbladder body ratios, serum markers (ALT, AST, ALP, TBA), histology (H&E, CK19/Hoechst, Masson's trichrome), and gene expression fold changes in $Atg5^{F/F}$ and $Atg5^{\Delta hep}$ mice treated with BAS.

excretion, which is reduced after ABX treatment, suggesting that GM maintained the total enterohepatic level of TBA in autophagy-deficient mice by an increased BA excretion from the intestine. The mechanism of this increased excretion may be related to the elevation of the BA-metabolizing bacteria because most excreted BA species are secondary and/or unconjugated BAs, which are produced through the action of bacteria.

Third, we present evidence that GM-mediated FXR activation in the ileum can induce FGF15 expression, thereby protecting mice from further liver damage caused by autophagy deficiency in the liver. Both the ABX and BAS treatments lead to dramatic inhibition of ileal FXR activity and significant decrease of FGF15 expression. Evidence from overexpression of FGF15 and inhibition of FGFR4 in the *Atg5*-deficient liver suggests that GM-mediated FGF15 expression at least partially protected *Atg5*$^{\Delta hep}$ mice from further liver damage by a FGF15-FGFR4 feedback signaling pathway.

We previously found that *Atg7* deletion induced more severe pathologic changes than *Atg5* deletion in the liver, which leads to different response to alcohol treatment.[35] In this study, we also observed that ABX treatment enhanced liver injury in *Atg5*$^{\Delta hep}$ but not obviously in *Atg7*$^{\Delta hep}$ mice, although increased BA pool and reduced ileal FXR activity after ABX treatment were observed in both *Atg5*$^{\Delta hep}$ and *Atg7*$^{\Delta hep}$ mice. It is possible that the protection effect from gut dysbiosis is overcome by additional hepatic phenotypes exerted by the more severe damage in the absence of *Atg7*, which sits on the upstream of Atg5 in the autophagy signaling pathway.

Gut Dysbiosis Can Be an Adaptive Response to Liver Injury

A number of studies had shown that gut dysbiosis contributes to the progress of liver disease, and correction of the dysbiosis may improve pathologic changes in the liver.[36–40] Among the detrimental effects of GM, "invasion" of the liver by the product of GM because of increased gut permeability is thought to be the major one.[4] Although the detrimental role of gut dysbiosis seems to be widely recognized, there is also evidence indicating a beneficial impact of GM on acute liver injury in mice. Enrichment of intestinal *Lactobacillus* was found in mice with liver injury induced by acute concanavalin A treatment, which can prevent further liver inflammation through activation of interleukin 22 production.[41] Furthermore, conflicting evidence supporting either a detrimental[42,43] or beneficial[14,44] effect of GM can be found for the liver injury in the

adenosine triphosphate–binding cassette, subfamily B (MDR/TAP), member 4 (*Mdr2*) knockout (*Mdr2*$^{-/-}$) mice.

In the present study, we have found GM are altered in *Atg5*$^{\Delta hep}$ mice. Surprisingly, ABX treatment enhanced *Atg5* deficiency-induced liver injury, clearly indicating a protective role of GM in *Atg5*$^{\Delta hep}$ mice. We further identified an increase of FXR activity and ileal FGF15 expression in *Atg5*$^{\Delta hep}$ mice, which is associated with the altered intestinal BA composition and the dysbiosis status of GM. Our findings demonstrate that FGF15 can be a beneficial feedback signal from gut dysbiosis attributed to hepatic autophagy deficiency.

In mice, FGF15 is induced by FXR activation in the ileum, and its human ortholog is FGF19.[18] FGF15/19 is required for the efficiency of SHP-mediated CYP7A1 repression and plays a critical role in repressing BA synthesis.[18] Conversely, decrease of intestinal level of BA by BAS can reduce ileal FGF15 expression in mice[26] and serum FGF19 levels in healthy humans.[45] Animal experiments have shown that FGF15 is essential for hepatic homeostasis, and overexpression of FGF15/19 in the liver has beneficial effects on multiple liver diseases including sclerosing cholangitis,[20] alcoholic fatty liver,[22] and NAFLD.[21,29] In addition to its functions in hepatic metabolism, FGF15 has also been shown to contribute to liver regeneration.[23,46,47] In humans, circulating FGF19 has been found to be increased in patients with biliary cirrhosis[48] and in patients with alcoholic hepatitis,[49] which is accompanied with inhibition of BA synthesis. Nevertheless, the function and cause of increased levels of circulating FGF19 remain unclear. Our current finding of the beneficial effects of FGF15-FGFR4 signaling in autophagy-deficient livers provides evidence that increase of FGF15/19 level in the setting of liver diseases can potentially be a protective mechanism via the gut-liver interaction.

Our study suggests that GM can adapt to metabolic changes in the liver and consequently activate feedback signaling, such as FXR-FGF15 signaling, in the gut to protect the liver from further damage. The present study also suggests caution should be exercised in the use of ABX during specific liver diseases to avoid potential detrimental effects, not because of reduced hepatic drug metabolism but because of disruption of beneficial gut-liver signaling.

Conclusion

In summary, the findings in our studies indicate a primary liver disease can lead to alteration of GM, which then

---

Figure 13. (*See previous page*). BAS reduced TBA pool but enhanced *Atg5* deficiency-induced liver injury. (*A*) Scheme of the BAS treatment. Water was given as control. (*B*) TBA levels in the indicated compartments were measured (n = 6–8/group). (*C*) Liver weight and gallbladder (Gal) weight were determined as percentage of body weight (n = 6–8/group). (*D*) Serum levels of ALT, AST, ALP, and TBA in mice after BAS treatment (n = 6–8/group). (*E*) Liver sections were subjected to H&E, anti-CK19, or Masson's trichrome staining. Percentage of positive area was quantified with ImageJ (anti-CK19 staining quantification, n = 3–4/group; Masson's trichrome staining quantification, n = 3–5/group). (*F* and *G*) Expression of genes related to BA metabolism in ileums (*F*) or in livers (*G*) was analyzed by qRT-PCR (n = 4–6/group). Data are shown as means ± SE. Groups with different lowercase letters had significant differences (*P* < .05). *Bsep* (*Abcb11*), bile salt export pump; *Cyp7a1*, cytochrome P450 7a1; *Mrp2* (*Abcc2*), multidrug resistance-associated protein 2; *Mrp3* (*Abcc3*), multidrug resistance-associated protein 3; *Mrp4* (*Abcc4*), multidrug resistance-associated protein 4; *Ntcp* (*Slc10a1*), Na/Taurocholate cotransporting polypeptide; *Oatp1* (*Slco1a1*), organic anion-transporting polypeptide 1.
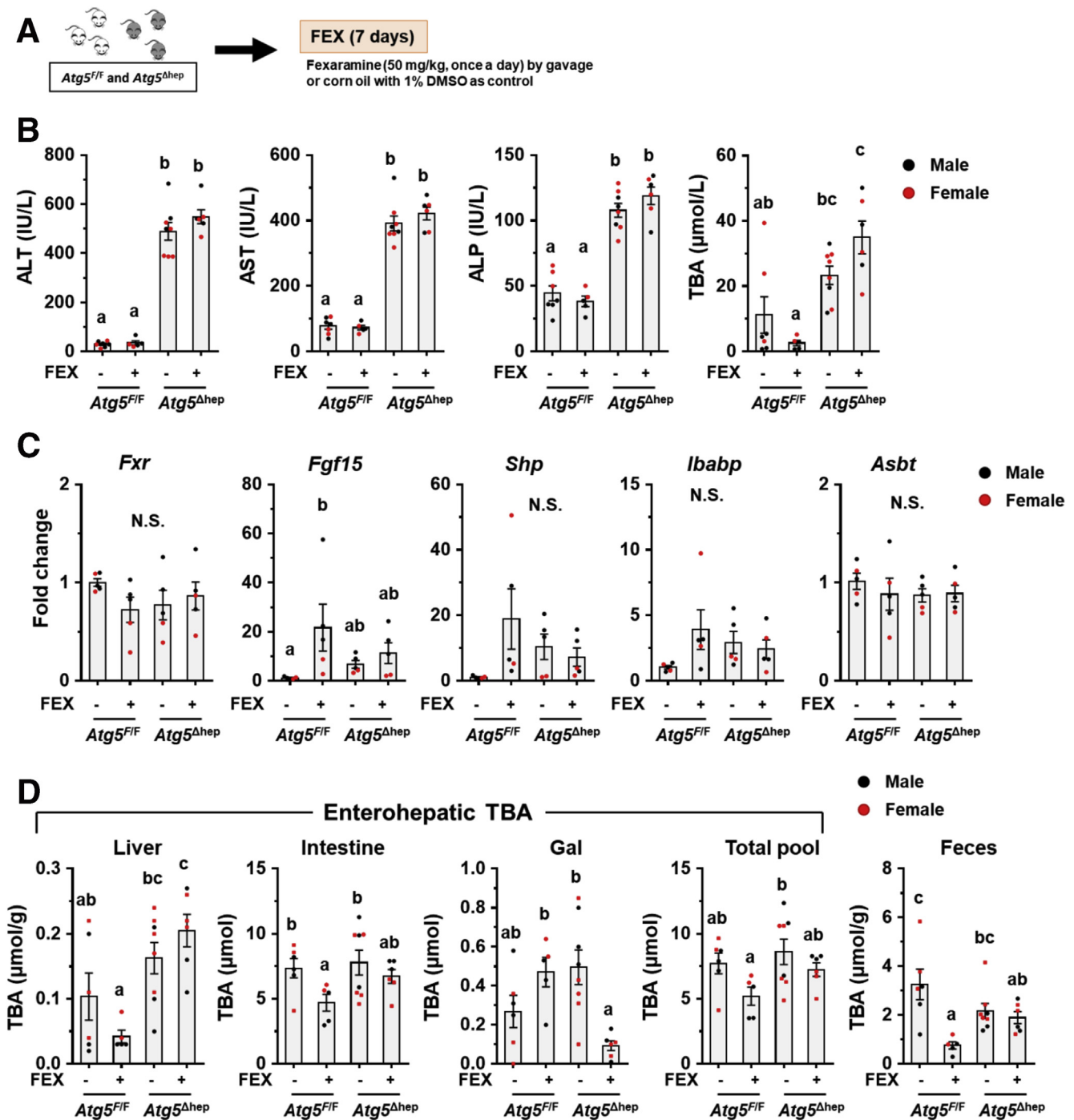
Figure 14. Intestine-specific FXR agonist activated ileal FXR in *Atg5^F/F* but not in *Atg5^Δhep* mice. (*A*) Scheme of the study using an intestine-specific FXR agonist, FEX. Solvent (1% dimethyl sulfoxide in corn oil) was given as the control. (*B*) Serum levels of ALT, AST, ALP, and TBA in mice after FEX treatment (n = 5–8). (*C*) Ileal expression of indicated genes was analyzed by qRT-PCR (n = 5). (*D*) TBA levels in the indicated compartments were measured (n = 5–8). Data are shown as means ± SE. Groups with different lowercase letters had significant differences (*P* < .05).

activates FXR-FGF15 feedback signaling through modulating the composition of intestinal BAs. Our results suggest that ABX treatment can exacerbate hepatic pathogenesis in *Atg5*-deficient livers by the reduction of FGF15 expression. Taken together, our present study demonstrates a protective role of gut dysbiosis in liver injury, which is associated with the FXR-FGF15-FGFR4 feedback signaling.
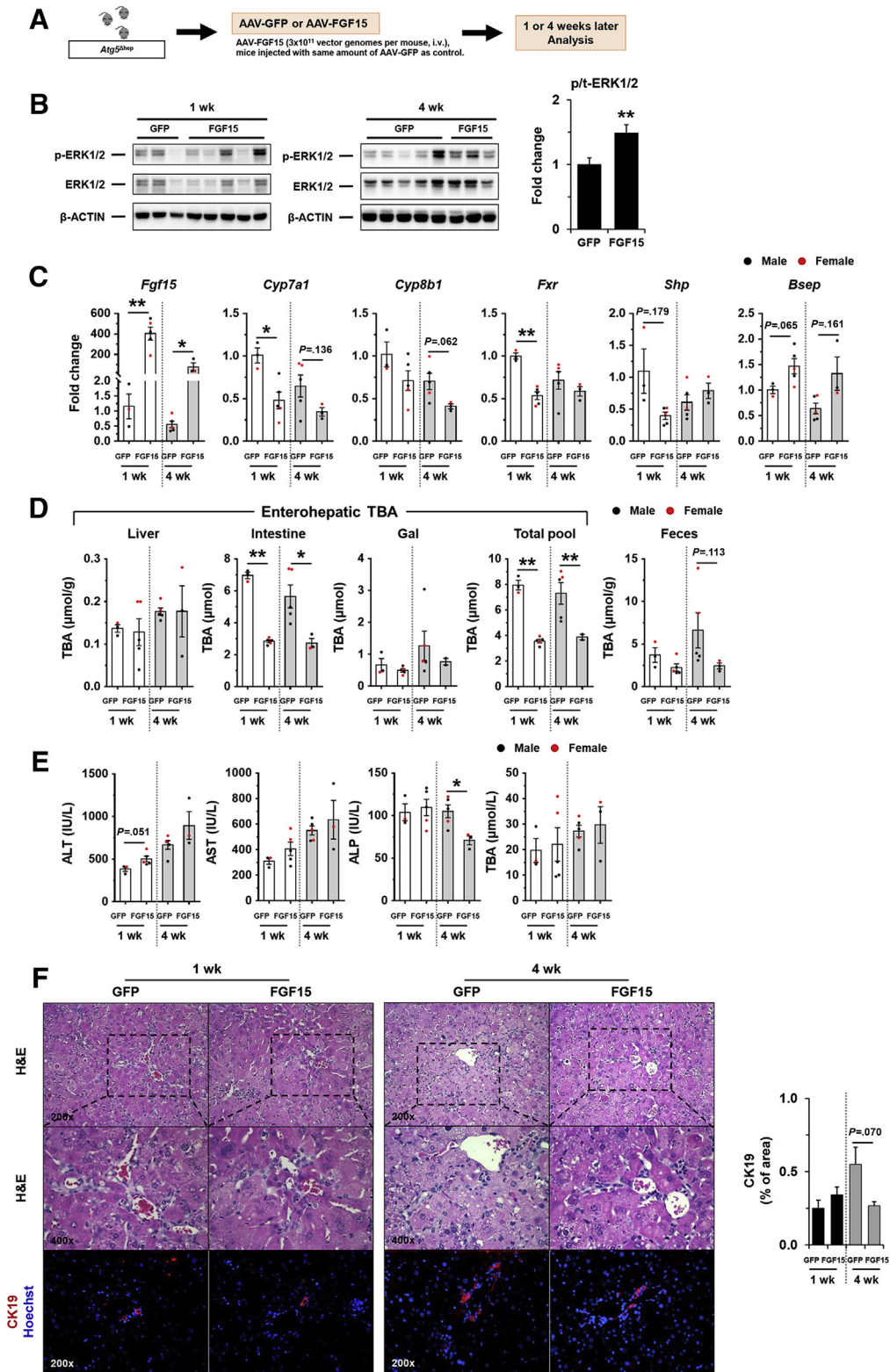
Figure 15. Overexpression of FGF15 attenuated pathologic features in *Atg5^Δhep* livers. (*A*) Scheme of the FGF15 over-expression study in mouse livers. (*B*) Expression of ERK1/2 in the liver was analyzed by immunoblotting assay and quantified by densitometry. Phosphorylation levels of ERK1/2 were normalized to those of the total protein levels and expressed as fold change of GFP group (n = 8/group). (*C*) Hepatic expression of indicated genes was analyzed by qRT-PCR (n = 3–5/group). Data were expressed as fold change of GFP for the 1-week group. (*D*) TBA levels in the indicated compartments were measured (n = 3–5/group). (*E*) Serum levels of ALT, AST, ALP, and TBA in mice after AAV injection (n = 3–5/group). (*F*) Liver sections were subjected to H&E, anti-CK19, or Masson's trichrome staining. Percentage of positive area was quantified with ImageJ (n = 3–5/group). Data are shown as means ± SE. **P* < .05, ***P* < .01. AAV, adeno-associated virus; *Bsep* (*Abcb11*), bile salt export pump; *Cyp7a1*, cytochrome P450 7a1; GFP, green fluorescence protein.
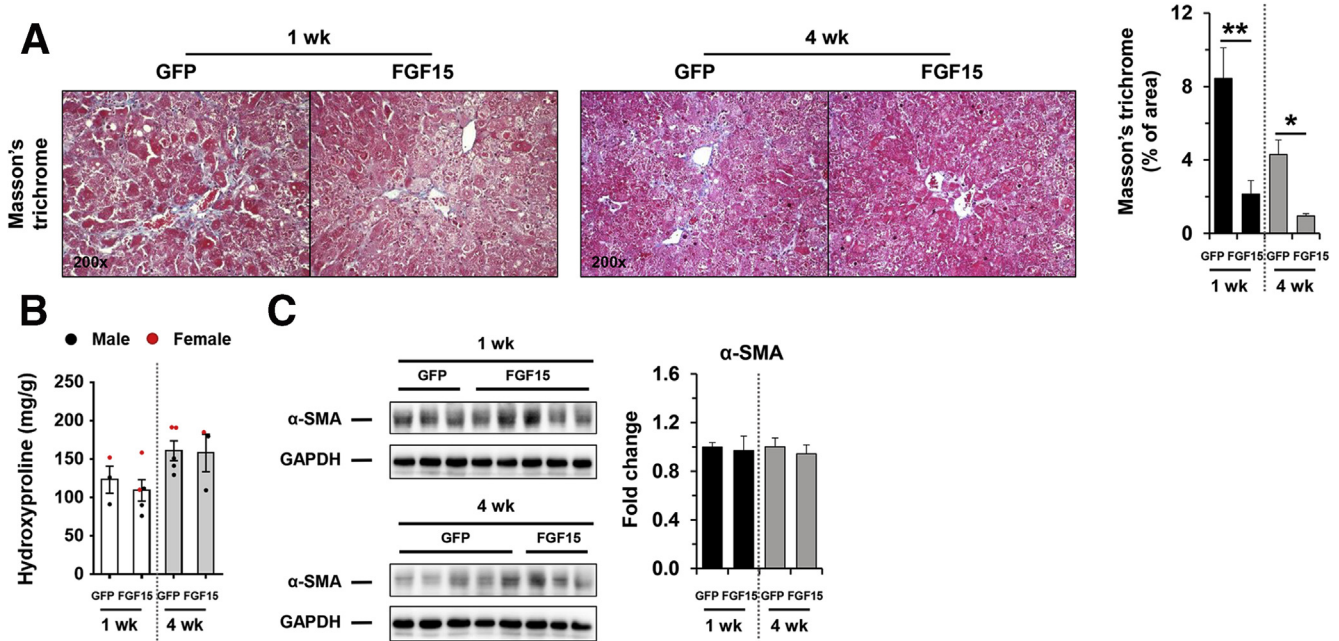
Figure 16. Effects of FGF15 on fibrosis in mouse livers. (*A*) Liver sections were subjected to Masson's trichrome staining. Percentage of positive area was quantified with ImageJ (n = 3–5). (*B*) Hepatic levels of hydroxyproline (n = 3–5). (*C*) Protein level of α-SMA in the liver was analyzed by immunoblotting assay and quantified by densitometry (n = 3–5). Data are shown as means ± SE. *P < .05, **P < .01. α-SMA, α-smooth muscle actin. GFP, green fluorescence protein.

Methods

Animals and Treatments

$Atg5^{F/F}$ mice ($B6.129S$-$Atg5tm1Myok$)[10] and $Atg7^{F/F}$ mice[12] had been reported in previous studies. $Atg5^{\Delta hep}$ and $Atg7^{\Delta hep}$ mice were created by cross $Atg5^{F/F}$ or $Atg7^{F/F}$ with the Alb:Cre transgenic mice (The Jackson Laboratory, Bar Harbor, ME), respectively. Mice were maintained on a 12-hour dark/12-hour light cycle with free access to food and water. Both male and female mice were used in the studies if not further addressed. Age- and sex-matched mice were randomly assigned to treatment or control group. For ABX treatment, mice (5 to 6 weeks old) were given ABX (0.5 g/L neomycin sulfate and 1 g/L ampicillin) in daily drinking water for 6 weeks. For BAS treatment, cholestyramine resin (2 g/kg) was mixed in water and given to 8- to 12-week-old mice twice a day by oral gavage for 5 days. Control groups were given a same volume of water. For FEX treatment, FEX was dissolved in dimethyl sulfoxide and further diluted in corn oil according to manufacturer's protocol. Mice (8 to 12 weeks old) were given 50 mg/kg FEX daily by oral gavage for 7 days. Control mice were given the same volume of corn oil containing the same amount of dimethyl sulfoxide. For adeno-associated virus (AAV8)-mediated overexpression of FGF15, $Atg5^{\Delta hep}$ mice (6 to 8 weeks old) were given 3 × 10^{11} vector genomes of AAV8-FGF15 per mouse by intravenous injection. Control mice were given AAV8-GFP. Mice were euthanized for further analysis 1 or 4 weeks later. For FGFR4 inhibitor treatment, BLU was dissolved in 0.5% methylcellulose/1% Tween 80 solution according to a previous study.[30] Mice (8 to 12 weeks old) were given 50 mg/kg BLU twice per day by oral gavage for 7 days. Control mice

were given the same volume of solvent. All animal experiments were approved by the Institutional Animal Care and Use Committee (IACUC) of Indiana University.

Antibodies and Chemicals

Antibodies and polymerase chain reaction primers used in this study are listed in Tables 1 and 2, respectively.

Fecal 16S rRNA Sequencing of Gut Microbial Communities

Mice were 6–26 weeks old when fecal samples were collected. For $Atg5^{\Delta hep}$ mice, fecal samples were collected from $Atg5^{F/F}$ and $Atg5^{\Delta hep}$ mice at 8 or 16 weeks old. For $Atg7^{\Delta hep}$ mice, fecal samples were collected from floxed $Atg7$ mice (heterozygous or homozygous, $Atg7^{WT}$) and $Atg7^{\Delta hep}$ mice. Both male and female mice were used and equally distributed in different genotypes. Fecal DNA was extracted from frozen fecal samples by using the E.Z.N.A. Stool DNA Kit (Omega Bio-Tek, Inc, Norcross, GA). All DNA samples were stored at –80°C before sequencing, which was performed by SeqMatic LLC (Fremont, CA) using Illumina (San Diego, CA) sequencing libraries. FASTQ data were processed by using the Qiime pipeline on Illumina's BaseSpace servers.

For 16S sequencing analysis, relative abundance of each bacteria was calculated. PCoA was performed by using multidimensional scaling function based on relative abundance at species level using SPSS for Windows 17.0 Software (SPSS, Inc, Chicago, IL). Heatmaps were generated by using Morpheus (https://software.broadinstitute.org/morpheus), and values in the heatmap were mapped to
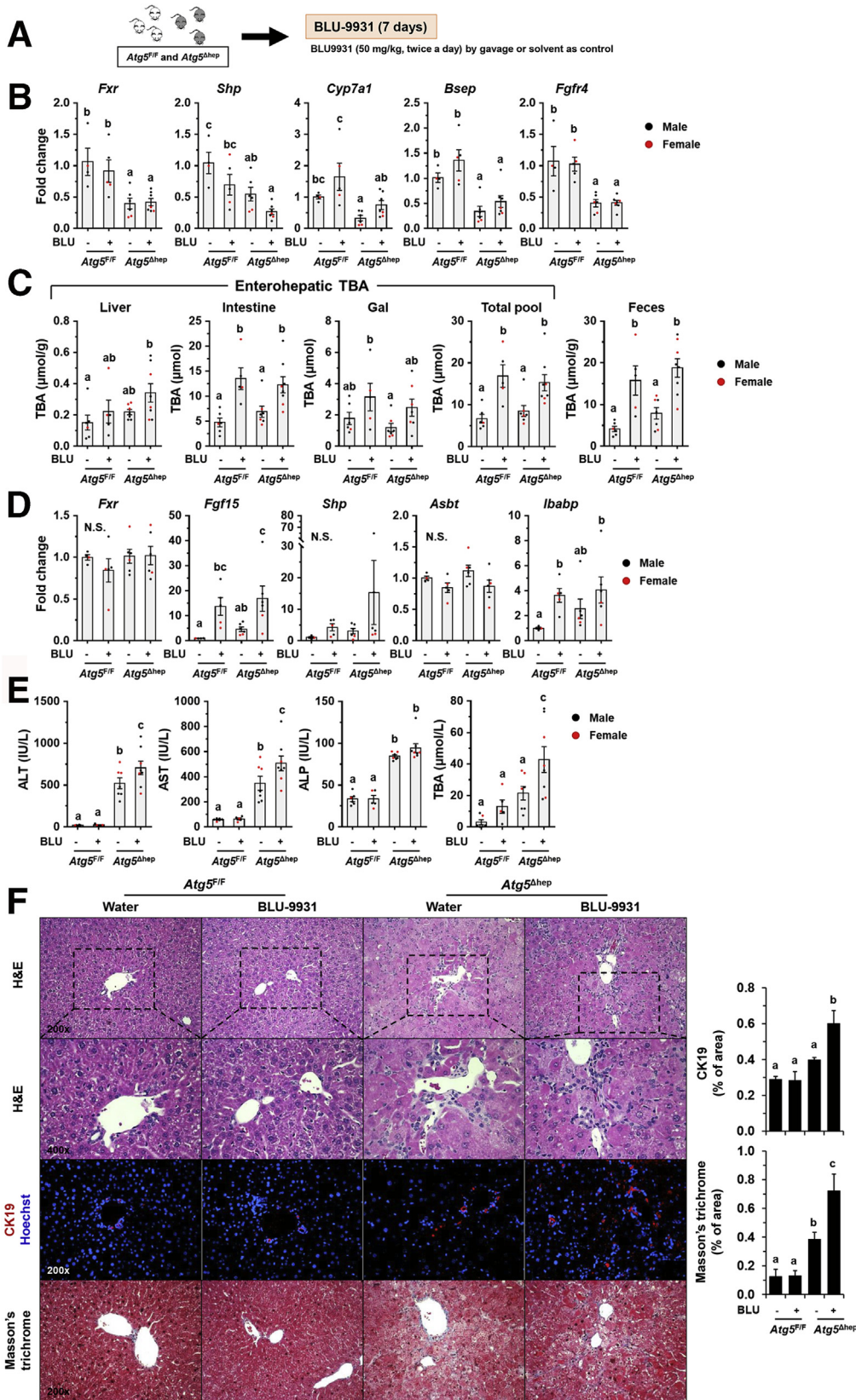
Figure 17. Inhibition of FGFR4 aggravated liver injury in *Atg5^Δhep* mice. (*A*) Scheme of treatment with FGFR4 inhibitor, Blu-9931 (BLU). Solvent (0.5% methylcellulose/1% Tween 80) was given as control. (*B*) Hepatic expression of indicated genes was analyzed by qRT-PCR (n = 4–7/group). (*C*) TBA levels in indicated compartments were measured (n = 6–8/group). (*D*) Ileal expression of indicated genes was analyzed by qRT-PCR (n = 4–6/group). (*E*) Serum levels of ALT, AST, ALP, and TBA in mice after BLU treatment (n = 6–8/group). (*F*) Liver sections were subjected to H&E, anti-CK19, or Masson's trichrome staining. Percentage of positive area was quantified with ImageJ (CK19 staining quantification, n = 3–6/group; Masson's trichrome staining quantification, n = 4–5/group). Data are shown as means ± SE. Groups with different lowercase letters had significant differences (*P* < .05). *Bsep* (*Abcb11*), bile salt export pump; N.S., no statistical significance.

Measurement of liver weight and serum ALT, AST, and ALP levels in *Atg5*-deficient livers with and without Blu-9931 (BLU) treatment. Results showed more significant effect of BLU treatment in male mice. Data are shown as means ± SE. *P <.05, **P < .01. N.S., no statistical significance.
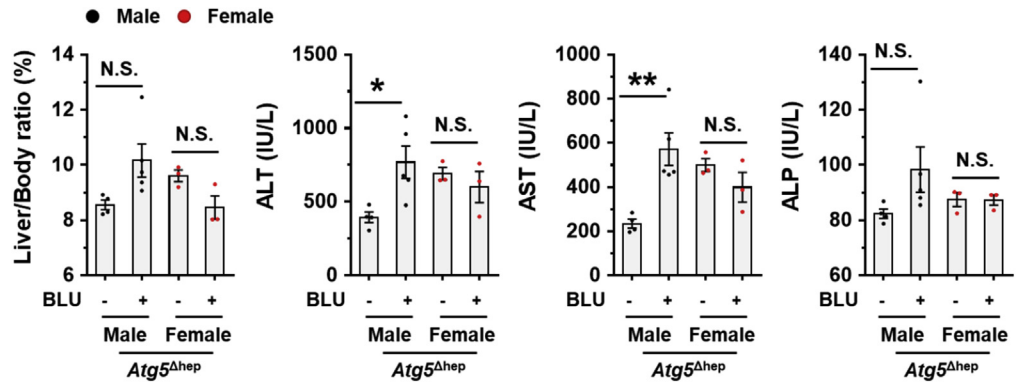
colors using the minimum and maximum of each row independently. The hierarchical cluster of each heatmap was constructed using one minus Pearson correlation method.

Serum Biochemistry Analysis

Serum levels of ALT, AST, and ALP were measured by using kits from Pointe Scientific (Canton, MI) according to the manufacturer's protocol. Serum TBAs were measured using the TBAs assay kit from Diazyme Laboratories, Inc (Poway, CA).
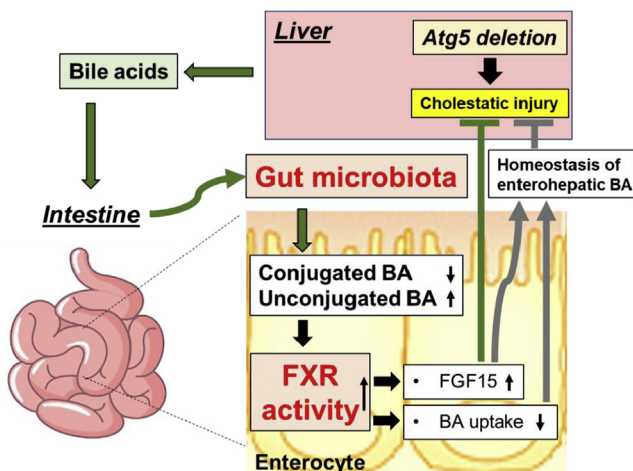
Tissue and Fecal TBA Content Analysis

Sample preparation and BA quantification were performed as in previous studies with modifications.[27] For the

Figure 19. GM-dependent FXR-FGF15 signaling improves hepatic presentation in *Atg5*-deficient mice. *Atg5* deficiency in the liver impairs autophagy process and BA homeostasis, which causes liver injury accompanied with cholestasis. Disruption of hepatic BA homeostasis altered the composition of BAs in the intestine and GM , which in turn affects BA composition in the intestine. The changes in intestinal BA composition activate ileal FXR and consequently induce FGF15 expression and reduce BA uptake in the intestine, both of which can improve the homeostasis of enterohepatic BA. Importantly, FGF15 is beneficial to the improvement of the liver injury induced by autophagy deficiency.

liver tissue, samples (100 mg) were homogenized in 1 mL of 90% ethanol and incubated at 55°C overnight. The lysates were centrifuged at 10,000 rpm for 10 minutes. Supernatant was used to measure BA concentration. The whole intestine (with its content) was homogenized in 5 mL water and was incubated at 55°C overnight after addition of 45 mL ethanol. One milliliter of the lysates was removed for centrifugation at 10,000 rpm for 10 minutes. An aliquot of the supernatant was diluted 5 times and measured for BA concentration. For BAs in the gallbladder, the entire organ was put in 1 mL of 90% ethanol. After the gallbladder was cut to release the bile, the samples were incubated at 55°C overnight. The lysates were centrifuged at 10,000 rpm for 10 minutes. An aliquot of the supernatant was diluted 50 times to measure the BA concentration. For fecal BA measurement, overnight-dried fecal samples (150–250 mg) were admixed with 1 mL of 95% EtOH and incubated at 55°C overnight. The lysates were centrifuged at 10,000 rpm for 10 minutes. An aliquot of the supernatant was diluted 10 times for BA quantification. The BA concentration of each diluted supernatants was measured by using the TBAs assay kit from Diazyme Laboratories, Inc.

Liver and Intestinal BA Composition Analysis

Liver and intestinal samples from male mice were used for BA profile analysis. BA analysis was by using a Biocrates Bile Acids Kit (Biocrates Life Science AG, Innsbruck, Austria). Samples were prepared according to the manufacturer's protocol with modifications. At least 30 mg of liver tissue was homogenized in 3-fold volume of extraction buffer (ethanol/phosphate buffer, 85:15 v/v). For intestine samples, they were homogenized in 3 mL phosphate-buffered saline (PBS), and then 17 mL of 100% ethanol was added to extract BAs. All samples were probe-sonicated for 3 bursts with 10 seconds each. Samples were chilled in an ice bath for at least 60 seconds between bursts. Homogenized samples were stored at –80°C. Further BA extraction and profile analysis were performed according to manufacturer's protocol in Center for Genomic and Computational Biology, Duke University. Sample pool quality controls were created using equal volumes of all liver and intestine samples respectively. BAs were identified by using Biocrates Me*t*IDQ software. A PCoA was performed for BAs using JMP Pro v14.0 software (SAS, Cary, NC).

Table 1. Antibody List

Antibody name	Company	Catalog #	Host
ATG12	Cell Signaling	2011	Rabbit
β-ACTIN	Cell Signaling	3700	Mouse
CK19	DSHB	TROMA-III	Rat
Phospho-ERK1/2 (Thr202/Tyr204)	Cell Signaling	4370	Rabbit
ERK1/2	Cell Signaling	9102	Rabbit
FGF15	Santa Cruz	sc-514647	Mouse
GAPDH	Novus biologicals	NB 300-221	Mouse
LC3B	Sigma	L7543	Rabbit
NQO1	Abcam	ab34173	Rabbit
P62/SQSTM1	Abnova	H00008878-M01	Mouse
α-SMA	Thermo	PA5-19465	Rabbit
β-TUBULIN	Cell Signaling	86298	Mouse

For BA composition analysis, results of analytes with more than 40% missing values were removed before statistical analysis. Missing values of the remaining results were then replaced with the limit of detection. Results from liver samples were calculated as nmoL/g or percentage of TBA level and were calculated as nmoL/whole intestine or percentage of TBA level from intestine samples. Heatmaps were generated using Morpheus (https://software.broadinstitute.org/morpheus), and values in the heatmap were mapped to colors using the minimum and maximum of each row independently. The hierarchical cluster of each heatmap was constructed using one minus Pearson correlation method.

Immunoblotting Analysis

The liver samples were homogenized in the radio immunoprecipitation assay buffer containing a protease cocktail and phosphatase inhibitors. Supernatant was collected after centrifugation at 12,000 rpm for 12 minutes. Protein concentration was determined by using BCA protein assay kit (Thermo Fisher Scientific-Pierce, Waltham, MA). The proteins were separated on a sodium dodecyl sulfate polyacrylamide gel electrophoresis. Proteins were transferred onto polyvinylidene fluoride membranes, which were then blocked with 5% bovine serum albumin or 5% skim milk for 1 hour at room temperature. Membranes were incubated with the appropriate primary antibody overnight and then washed with TBST (Tris-buffered saline, 0.1% Tween 20) before being incubated with the horseradish peroxidase–coupled secondary antibodies at room temperature. Protein bands were detected by using enhanced chemiluminescence kit (Thermo Fisher Scientific-Pierce). The images were taken digitally with a BioRad ChemiDoc Image System (BioRad, Hercules, CA). Densitometry was measured by using the companion software, and the values were normalized to those of β-tubulin, β-actin, or glyceraldehyde-3-phosphate dehydrogenase (GAPDH), which were then converted to fold change of the control.

RNA Isolation and Quantitative Real-Time PCR Analysis

Total RNA was prepared from liver samples using Gene-TET RNA purification kit (Thermo Fisher Scientific, Grand Island, NY) according to manufacturer's protocols. Complementary DNA (cDNA) was synthesized using Oligo dT primers and an M-MLV reverse transcriptase system (Life Technologies-Thermo Fisher Scientific). Quantitative real-time polymerase chain reaction (qRT-PCR) analysis was performed on a QuantStudio 3 Real-Time PCR System (Life Technologies-Applied Biosystems, Waltham, MA) using SYBR Green master mixes (Life Technologies-Applied Biosystems). All qRT-PCR results were normalized to the level of β-actin, and the gene expression was calculated using the $2^{-\Delta\Delta Ct}$ method.

Histologic Study

Liver or ileum samples were rinsed with PBS and fixed in 10% formalin overnight. Samples were further fixed in 70% ethanol and processed as paraffin-embedded blocks. The paraffin-embedded liver tissues were sectioned and stained with H&E or Mason's trichrome C. The paraffin-embedded ileum tissues were sectioned, and immunohistochemical staining was performed with FGF15 antibody. Photomicrographs were taken using a Nikon (Tokyo, Japan) Eclipse E200 light microscope equipped with a SPOT RT Slider color digital camera (Diagnostic Instruments, Inc, Sterling Heights, MI). Area with positive Mason's trichrome C staining was quantified by using ImageJ software (National Institutes of Health, Bethesda, MD); at least 4 random fields of each section from each mouse liver were used for quantification.[50]

Immunofluorescence Microscopy

Paraffin sections were subjected to antigen retrieval treatment using the Citrate buffer (0.01 mol/L, pH 6.0) after deparaffinization. Slides were blocked with 5% goat serum in PBS containing 0.1% Triton X (PBS-Tx) for 1 hour and then incubated with primary antibodies diluted

Table 2. Primer List

Gene name	equence (forward)	Sequence (reverse)
Actin	5′-ACTATTGGCAACGAGCGGTT-3′	5′-CAGGATTCCATACCCAAGAAGGA-3′
Akr1d1	5′-CTCATTGGGCTTGGAACCTA-3′	5′-CATTGATGGGACATGCTCTG-3′
Asbt (Slc10a2)	5′-CGACATGGACCTCAGTGTTAG-3′	5′-CAACCCACATCTTGGTGTAGA-3′
Baat	5′-GTCCTTTTCCAGGGGTCATT-3′	5′-CCAGAGCTAAGGTGGCAAAG -3′
Bsep (Abcb11)	5′-CTGCCAAGGATGCTAATGCA-3′	5′-CGATGGCTACCCTTTGCTTCT-3′
Cyp27a1	5′-GCCTCACCTATGGGATCTTCA-3′	5′-TCAAAGCCTGACGCAGATG-3′
Cyp7a1	5′-AACAACCTGCCAGTACTAGATAGC-3′	5′-GTGTAGAGTGAAGTCCTCCTTAGC-3′
Cyp7b1	5′-CAGCTATGTTCTGGGCAATG-3′	5′-TCGGATGATGCTGGAGTATG-3′
Cyp8b1	5′-AGTACACATGGACCCCGACATC-3′	5′-GGGTGCCATCCGGGTTGAG-3′
Fgfr4	5′-CTGCCAGAGGAAGACCTCAC-3′	5′-GTAGTGGCCACGGATGACTT-3′
Fgf15	5′-ATGGCGAGAAAGTGGAACG -3′	5′-CTGACACAGACTGGGATTGCT-3′
Fxr (Nr1h4)	5′-GGCCTCTGGGTACCACTACA-3′	5′-TGTACACGGCGTTCTTGGTA-3′
Gstm1	5′-ACTTGATTGATGGGGCTCAC-3′	5′-TCTCCAAAATGTCCACACGA-3′
Ibabp	5′-CCCCAACTATCACCAGACTTC-3′	5′-ACATCCCCGATGGTGGAGAT-3′
Mdr1a (Abcb1)	5′-AAAGGCTCTACGACCCCCTA-3′	5′-CCTGACTCACCACACCAATG-3′
Mrp2 (Abcc2)	5′-GCACTGTAGGCTCTGGGAAG-3′	5′-TGCTGAGGGACGTAGGCTAT-3′
Mrp3 (Abcc3)	5′-GGACTTCCAGTGCTCAGAGG-3′	5′-AGCTGTGGCCTCGTCTAAAA-3′
Mrp4 (Abcc4)	5′-TGTTTGATGCACACCAGGAT-3′	5′-GACAAACATGGCACAGATGG-3′
Nqo1	5′-GCACTGATCGTACTGGCTCA-3′	5′-CATGGCATAGAGGTCCGACT-3′
Ntcp (Slc10a1)	5′-CACCATGGAGTTCAGCAAGA-3′	5′-CCAGAAGGAAAGCACTGAGG-3′
Ost-α (Slc51A)	5′-GTCTCAAGTGATGAACTGCCA-3′	5′-TTGAGTGCTGAGTCCAGGTC-3′
Ost-β (Slc51B)	5′-GTATTTTCGTGCAGAAGATGCG-3′	5′-TTTCTGTTTGCCAGGATGCTC-3′
Oatp1 (Slco1a1)	5′-ATCCAGTGTGTGGGGACAAT-3′	5′-GCAGCTGCAATTTTGAAACA-3′
Shp	5′-CTGGTTGAGCGCCTGAGAC-3′	5′-CTGCCTGGATGCCCTTTATC -3′

in 1% bovine serum albumin/PBS-Tx overnight at 4°C. Sections were washed with PBS, followed by incubation with fluorochrome-conjugated secondary antibodies. Hoechst 33342 was used for nucleus staining. Images were obtained by using a Nikon Eclipse TE 200 epi-immunofluorescence microscope and the companion NIS-Elements AR3.2 software. Quantification was performed by using ImageJ software; at least 4 random fields of each section from each mouse liver were analyzed.

Statistical Analysis

The 16S sequencing data were represented as median with interquartile range. All the other data were represented as means with standard errors (SEs). For 16S sequencing data, Mann-Whitney test was performed to identify bacteria with significantly different proportions between $Atg5^{\Delta hep}$ and sex- and age-matched $Atg5^{F/F}$ mice. For all other data, to determine statistical significance, Student t test was used to determine differences between 2 groups. Differences among more than 2 treatment groups were determined by using one-way analysis of variance followed by Duncan's post hoc test. Results were considered statistically significant for P value $<.05$. Statistical analyses were performed by using SPSS for Windows 17.0 Software (SPSS, Inc).

References

1. Nicholson JK, Holmes E, Kinross J, Burcelin R, Gibson G, Jia W, Pettersson S. Host-gut microbiota metabolic interactions. Science 2012;336:1262–1267.
2. Schnabl B, Brenner DA. Interactions between the intestinal microbiome and liver diseases. Gastroenterology 2014;146:1513–1524.
3. Bajaj JS. Alcohol, liver disease and the gut microbiota. Nat Rev Gastroenterol Hepatol 2019;16:235–246.
4. Tripathi A, Debelius J, Brenner DA, Karin M, Loomba R, Schnabl B, Knight R. The gut-liver axis and the intersection with the microbiome. Nat Rev Gastroenterol Hepatol 2018;15:397–411.
5. Li T, Chiang JY. Bile acids as metabolic regulators. Curr Opin Gastroenterol 2015;31:159–165.
6. Jia W, Xie G, Jia W. Bile acid-microbiota crosstalk in gastrointestinal inflammation and carcinogenesis. Nat Rev Gastroenterol Hepatol 2018;15:111–128.
7. Sabino J, Vieira-Silva S, Machiels K, Joossens M, Falony G, Ballet V, Ferrante M, Van Assche G, Van der Merwe S, Vermeire S, Raes J. Primary sclerosing cholangitis is characterised by intestinal dysbiosis independent from IBD. Gut 2016;65:1681–1689.
8. Levine B, Kroemer G. Biological functions of autophagy genes: a disease perspective. Cell 2019;176:11–42.
9. Komatsu M, Waguri S, Koike M, Sou YS, Ueno T, Hara T, Mizushima N, Iwata J, Ezaki J, Murata S, Hamazaki J,

Nishito Y, Iemura S, Natsume T, Yanagawa T, Uwayama J, Warabi E, Yoshida H, Ishii T, Kobayashi A, Yamamoto M, Yue Z, Uchiyama Y, Kominami E, Tanaka K. Homeostatic levels of p62 control cytoplasmic inclusion body formation in autophagy-deficient mice. Cell 2007;131:1149–1163.

10. Takamura A, Komatsu M, Hara T, Sakamoto A, Kishi C, Waguri S, Eishi Y, Hino O, Tanaka K, Mizushima N. Autophagy-deficient mice develop multiple liver tumors. Genes Dev 2011;25:795–800.

11. Khambu B, Li T, Yan S, Yu C, Chen X, Goheen M, Li Y, Lin J, Cummings OW, Lee YA, Friedman S, Dong Z, Feng GS, Wu S, Yin XM. Hepatic autophagy deficiency compromises farnesoid X receptor functionality and causes cholestatic injury. Hepatology 2019;69:2196–2213.

12. Komatsu M, Kurokawa H, Waguri S, Taguchi K, Kobayashi A, Ichimura Y, Sou YS, Ueno I, Sakamoto A, Tong KI, Kim M, Nishito Y, Iemura S, Natsume T, Ueno T, Kominami E, Motohashi H, Tanaka K, Yamamoto M. The selective autophagy substrate p62 activates the stress responsive transcription factor Nrf2 through inactivation of Keap1. Nat Cell Biol 2010;12:213–223.

13. Ni HM, Woolbright BL, Williams J, Copple B, Cui W, Luyendyk JP, Jaeschke H, Ding WX. Nrf2 promotes the development of fibrosis and tumorigenesis in mice with defective hepatic autophagy. J Hepatol 2014; 61:617–625.

14. Sayin SI, Wahlstrom A, Felin J, Jantti S, Marschall HU, Bamberg K, Angelin B, Hyotylainen T, Oresic M, Backhed F. Gut microbiota regulates bile acid metabolism by reducing the levels of tauro-beta-muricholic acid, a naturally occurring FXR antagonist. Cell Metab 2013;17:225–235.

15. Ridlon JM, Kang DJ, Hylemon PB. Bile salt biotransformations by human intestinal bacteria. J Lipid Res 2006;47:241–259.

16. Wahlstrom A, Sayin SI, Marschall HU, Backhed F. Intestinal crosstalk between bile acids and microbiota and its impact on host metabolism. Cell Metab 2016;24:41–50.

17. Urdaneta V, Casadesus J. Interactions between bacteria and bile salts in the gastrointestinal and hepatobiliary tracts. Front Med (Lausanne) 2017;4:163.

18. Kliewer SA, Mangelsdorf DJ. Bile acids as hormones: the FXR-FGF15/19 pathway. Dig Dis 2015;33:327–331.

19. Gadaleta RM, Moschetta A. Metabolic messengers: fibroblast growth factor 15/19. Nature Metabolism 2019; 1:588–594.

20. Zhou M, Learned RM, Rossi SJ, DePaoli AM, Tian H, Ling L. Engineered fibroblast growth factor 19 reduces liver injury and resolves sclerosing cholangitis in Mdr2-deficient mice. Hepatology 2016;63:914–929.

21. Zhou M, Luo J, Chen M, Yang H, Learned RM, DePaoli AM, Tian H, Ling L. Mouse species-specific control of hepatocarcinogenesis and metabolism by FGF19/FGF15. J Hepatol 2017;66:1182–1192.

22. Hartmann P, Hochrath K, Horvath A, Chen P, Seebauer CT, Llorente C, Wang L, Alnouti Y, Fouts DE, Starkel P, Loomba R, Coulter S, Liddle C, Yu RT, Ling L, Rossi SJ, DePaoli AM, Downes M, Evans RM, Brenner DA, Schnabl B. Modulation of the intestinal bile

acid/farnesoid X receptor/fibroblast growth factor 15 axis improves alcoholic liver disease in mice. Hepatology 2018;67:2150–2166.

23. Kong B, Sun R, Huang M, Chow MD, Zhong XB, Xie W, Lee YH, Guo GL. Fibroblast growth factor 15-dependent and bile acid-independent promotion of liver regeneration in mice. Hepatology 2018;68:1961–1976.

24. Dawson PA. Role of the intestinal bile acid transporters in bile acid and drug disposition. Handb Exp Pharmacol 2011;201:169–203.

25. Out C, Groen AK, Brufau G. Bile acid sequestrants: more than simple resins. Curr Opin Lipidol 2012;23:43–55.

26. Fuchs CD, Paumgartner G, Mlitz V, Kunczer V, Halilbasic E, Leditznig N, Wahlstrom A, Stahlman M, Thuringer A, Kashofer K, Stojakovic T, Marschall HU, Trauner M. Colesevelam attenuates cholestatic liver and bile duct injury in Mdr2(-/-) mice by modulating composition, signalling and excretion of faecal bile acids. Gut 2018;67:1683–1691.

27. Pathak P, Xie C, Nichols RG, Ferrell JM, Boehme S, Krausz KW, Patterson AD, Gonzalez FJ, Chiang JYL. Intestine farnesoid X receptor agonist and the gut microbiota activate G-protein bile acid receptor-1 signaling to improve metabolism. Hepatology 2018; 68:1574–1588.

28. Luo J, Ko B, Elliott M, Zhou M, Lindhout DA, Phung V, To C, Learned RM, Tian H, DePaoli AM, Ling L. A nontumorigenic variant of FGF19 treats cholestatic liver diseases. Sci Transl Med 2014;6:247ra100.

29. Alvarez-Sola G, Uriarte I, Latasa MU, Fernandez-Barrena MG, Urtasun R, Elizalde M, Barcena-Varela M, Jimenez M, Chang HC, Barbero R, Catalan V, Rodriguez A, Fruhbeck G, Gallego-Escuredo JM, Gavalda-Navarro A, Villarroya F, Rodriguez-Ortigosa CM, Corrales FJ, Prieto J, Berraondo P, Berasain C, Avila MA. Fibroblast growth factor 15/19 (FGF15/19) protects from diet-induced hepatic steatosis: development of an FGF19-based chimeric molecule to promote fatty liver regeneration. Gut 2017;66:1818–1828.

30. Hagel M, Miduturu C, Sheets M, Rubin N, Weng W, Stransky N, Bifulco N, Kim JL, Hodous B, Brooijmans N, Shutes A, Winter C, Lengauer C, Kohl NE, Guzi T. First selective small molecule inhibitor of FGFR4 for the treatment of hepatocellular carcinomas with an activated FGFR4 signaling pathway. Cancer Discov 2015;5:424–437.

31. Chiang JYL, Ferrell JM. Bile acids as metabolic regulators and nutrient sensors. Annu Rev Nutr 2019; 39:175–200.

32. Kummen M, Hov JR. The gut microbial influence on cholestatic liver disease. Liver Int 2019;39:1186–1196.

33. Little R, Wine E, Kamath BM, Griffiths AM, Ricciuto A. Gut microbiome in primary sclerosing cholangitis: a review. World J Gastroenterol 2020;26:2768–2780.

34. Chen W, Wei Y, Xiong A, Li Y, Guan H, Wang Q, Miao Q, Bian Z, Xiao X, Lian M, Zhang J, Li B, Cao Q, Fan Z, Zhang W, Qiu D, Fang J, Gershwin ME, Yang L, Tang R, Ma X. Comprehensive analysis of serum and fecal bile acid profiles and interaction with gut microbiota in primary biliary cholangitis. Clin Rev Allergy Immunol 2020; 58:25–38.

35. Yan S, Zhou J, Chen X, Dong Z, Yin XM. Diverse consequences in liver injury in mice with different autophagy functional status treated with alcohol. Am J Pathol 2019; 189:1744–1762.

36. De Minicis S, Rychlicki C, Agostinelli L, Saccomanno S, Candelaresi C, Trozzi L, Mingarelli E, Facinelli B, Magi G, Palmieri C, Marzioni M, Benedetti A, Svegliati-Baroni G. Dysbiosis contributes to fibrogenesis in the course of chronic liver injury in mice. Hepatology 2014; 59:1738–1749.

37. Jena PK, Sheng L, Liu HX, Kalanetra KM, Mirsoian A, Murphy WJ, French SW, Krishnan VV, Mills DA, Wan YY. Western diet-induced dysbiosis in farnesoid X receptor knockout mice causes persistent hepatic inflammation after antibiotic treatment. Am J Pathol 2017; 187:1800–1813.

38. Ferrere G, Wrzosek L, Cailleux F, Turpin W, Puchois V, Spatz M, Ciocan D, Rainteau D, Humbert L, Hugot C, Gaudin F, Noordine ML, Robert V, Berrebi D, Thomas M, Naveau S, Perlemuter G, Cassard AM. Fecal microbiota manipulation prevents dysbiosis and alcohol-induced liver injury in mice. J Hepatol 2017; 66:806–815.

39. Grander C, Adolph TE, Wieser V, Lowe P, Wrzosek L, Gyongyosi B, Ward DV, Grabherr F, Gerner RR, Pfister A, Enrich B, Ciocan D, Macheiner S, Mayr L, Drach M, Moser P, Moschen AR, Perlemuter G, Szabo G, Cassard AM, Tilg H. Recovery of ethanol-induced Akkermansia muciniphila depletion ameliorates alcoholic liver disease. Gut 2018;67:891–901.

40. Chen P, Starkel P, Turner JR, Ho SB, Schnabl B. Dysbiosis-induced intestinal inflammation activates tumor necrosis factor receptor I and mediates alcoholic liver disease in mice. Hepatology 2015;61:883–894.

41. Nakamoto N, Amiya T, Aoki R, Taniki N, Koda Y, Miyamoto K, Teratani T, Suzuki T, Chiba S, Chu PS, Hayashi A, Yamaguchi A, Shiba S, Miyake R, Katayama T, Suda W, Mikami Y, Kamada N, Ebinuma H, Saito H, Hattori M, Kanai T. Commensal Lactobacillus controls immune tolerance during acute liver injury in mice. Cell Rep 2017;21:1215–1226.

42. Tedesco D, Thapa M, Chin CY, Ge Y, Gong M, Li J, Gumber S, Speck P, Elrod EJ, Burd EM, Kitchens WH, Magliocca JF, Adams AB, Weiss DS, Mohamadzadeh M, Grakoui A. Alterations in intestinal microbiota lead to production of interleukin 17 by intrahepatic gammadelta T-cell receptor-positive cells and pathogenesis of cholestatic liver disease. Gastroenterology 2018; 154:2178–2193.

43. Liao L, Schneider KM, Galvez EJC, Frissen M, Marschall HU, Su H, Hatting M, Wahlstrom A, Haybaeck J, Puchas P, Mohs A, Peng J, Bergheim I, Nier A, Hennings J, Reissing J, Zimmermann HW, Longerich T, Strowig T, Liedtke C, Cubero FJ, Trautwein C. Intestinal dysbiosis augments liver disease progression via NLRP3 in a murine model of primary sclerosing cholangitis. Gut 2019;68:1477–1492.

44. Tabibian JH, O'Hara SP, Trussoni CE, Tietz PS, Splinter PL, Mounajjed T, Hagey LR, LaRusso NF. Absence of the intestinal microbiota exacerbates hepatobiliary disease in a murine model of primary sclerosing cholangitis. Hepatology 2016;63:185–196.

45. Lundasen T, Galman C, Angelin B, Rudling M. Circulating intestinal fibroblast growth factor 19 has a pronounced diurnal variation and modulates hepatic bile acid synthesis in man. J Intern Med 2006;260:530–536.

46. Uriarte I, Fernandez-Barrena MG, Monte MJ, Latasa MU, Chang HC, Carotti S, Vespasiani-Gentilucci U, Morini S, Vicente E, Concepcion AR, Medina JF, Marin JJ, Berasain C, Prieto J, Avila MA. Identification of fibroblast growth factor 15 as a novel mediator of liver regeneration and its application in the prevention of post-resection liver failure in mice. Gut 2013;62:899–910.

47. Kong B, Huang J, Zhu Y, Li G, Williams J, Shen S, Aleksunes LM, Richardson JR, Apte U, Rudnick DA, Guo GL. Fibroblast growth factor 15 deficiency impairs liver regeneration in mice. Am J Physiol Gastrointest Liver Physiol 2014;306:G893–G902.

48. Li Z, Lin B, Lin G, Wu Y, Jie Y, Li X, Ko B, Chong Y, Luo J. Circulating FGF19 closely correlates with bile acid synthesis and cholestasis in patients with primary biliary cirrhosis. PLoS One 2017;12:e0178580.

49. Brandl K, Hartmann P, Jih LJ, Pizzo DP, Argemi J, Ventura-Cots M, Coulter S, Liddle C, Ling L, Rossi SJ, DePaoli AM, Loomba R, Mehal WZ, Fouts DE, Lucey MR, Bosques-Padilla F, Mathurin P, Louvet A, Garcia-Tsao G, Verna EC, Abraldes JG, Brown RS Jr, Vargas V, Altamirano J, Caballeria J, Shawcross D, Starkel P, Ho SB, Bataller R, Schnabl B. Dysregulation of serum bile acids and FGF19 in alcoholic hepatitis. J Hepatol 2018;69:396–405.

50. Kennedy DJ, Vetteth S, Periyasamy SM, Kanj M, Fedorova L, Khouri S, Kahaleh MB, Xie Z, Malhotra D, Kolodkin NI, Lakatta EG, Fedorova OV, Bagrov AY, Shapiro JI. Central role for the cardiotonic steroid marinobufagenin in the pathogenesis of experimental uremic cardiomyopathy. Hypertension 2006;47:488–495.

Correspondence
Address correspondence to: Xiao-Ming Yin, MD, PhD, Department of Pathology and Laboratory Medicine, Tulane University School of Medicine, New Orleans, Louisiana 70112. e-mail: xmyin@tulane.edu; fax: (504) 988-7389.

CRediT Authorship Contributions
Shengmin Yan (Conceptualization: Supporting; Data curation: Lead; Formal analysis: Lead; Investigation: Lead; Methodology: Lead; Writing – original draft: Lead; Writing – review & editing: Equal),
   Bilon Khambu (Formal analysis: Supporting; Investigation: Supporting; Methodology: Supporting),
   Xiaoyun Chen (Investigation: Supporting; Methodology: Supporting)
   Zheng Dong (Investigation: Supporting; Methodology: Supporting)
   Grace Guo (Investigation: Supporting; Resources: Supporting; Writing – review & editing: Supporting)
   Xiao-Ming Yin, MD, PhD (Conceptualization: Lead; Data curation: Support; Formal analysis: Support; Funding acquisition: Lead; Project administration: Lead; Resources: Lead; Supervision: Lead; Writing – original draft: Lead; Writing – review & editing: Lead)

Conflicts of interest
The authors disclose no conflicts.